Positron Annihilation in Noble Gas Bubbles in Metals

Jensen, K. O.

Publication date:
1987

Document Version
Publisher's PDF, also known as Version of record

Risø-M-2648

RISØ

Risø-M-2648

Positron Annihilation in Noble Gas Bubbles in Metals

Kjeld Ole Jensen

Risø National Laboratory, DK-4000 Roskilde, Denmark
November 1987

RISØ-M-2648

POSITRON ANNIHILATION IN NOBLE GAS BUBBLES IN METALS

Kjeld Ole Jensen

Abstract. An experimental and theoretical investigation of positron annihilation in noble gas bubbles in metals is presented.

A theoretical treatment of atomic structure and positron states in noble gas bubbles has been made. The Al-He and Cu-Kr systems are considered as specific examples. For large bubbles (radii above a few tens of A) a calculational scheme is developed combining molecular dynamics results for the metal-noble gas interface with positron calculations. It is demonstrated that a positron is trapped at the surface of a noble gas bubble, i.e. at the metal-gas interface, and relationships between gas density and positron lifetime were obtained for the systems considered. In the molecular dynamics simulations a trend towards close-packed layer-by-layer ordering of the gas atoms close to the metal-gas interface is found even in the cases, where the bulk gas is in a fluid phase. The positron state calculations also cover the case of adsorbed noble gas layers at surfaces. For small vacancy-noble gas clusters complementary positron results obtained with the calculational method developed by Puska and Nieminen are presented.

(continues)

November 1987
Forskningscenter Risø, DK-4000 Roskilde, Danmark

(continued)

Aluminium samples containing He bubbles produced by 600 MeV proton irradiation at temperatures in the range 375-728 K were investigated experimentally by positron annihilation using both the positron lifetime and angular correlation techniques. The samples irradiated below 485 K were studied both in the as-irradiated state and after annealing at temperatures up to 873 K. Evaluation of bubble parameters, i.e. the gas density inside bubbles and the average bubble size and concentration, were made from positron lifetime results employing the theoretical relation between positron lifetime and He density in bubbles and a semi-empirical relation between positron specific trapping rate and cavity radius. The results are consistent with determinations of bubble parameters by other experimental methods. In addition one-dimensional angular correlations curves for He bubbles as a function of He density are determined.

For the samples proton-irradiated above 655 K a very narrow component (full-width-at-half-maximum about 1.6 mrad) is present in the angular correlation spectra. This component is interpreted to be due to a positronium-like positron state in the He bubbles. The width of the narrow component indicates the state not to be free positronium in the bubble interior but a positronium-like state at the bubble surfaces. The Ps-like state is attributed to the presence of impurity atoms, possibly Na, at the surfaces of the bubbles.

Experimental positron lifetime results for Cu and Ni containing high concentrations of Kr are briefly discussed. Positron estimates of Kr densities inside the Kr bubbles present in the samples based on the theoretical results are consistent with independent estimates. Measurement of positron lifetimes as a function of temperature for the Cu-Kr samples after annealing close to the Cu melting point demonstrates the effect of Kr adsorption at the surfaces of the large bubbles present in the samples on the positron lifetime in the bubbles.

This report has been submitted to the University of Aarhus in partial fulfilment of the requirements for obtaining the lic. scient. (Ph.D.) degree.

Kjeld Ole Jensen

Metallurgy Department, Risø National Laboratory, DK-4000 Roskilde, Denmark.

Present address:
School of Mathematics and Physics, University of East Anglia, Norwich NR4 7TJ, UK

ISBN 87-550-1325-2
ISSN 0418-6435

CONTENTS.

APPENDICES (Not included in the present report):

PAPER I: 'Helium bubbles in aluminium studies by positron annihilation: Determination of bubble parameters.', Kjeld O. Jensen, M. Eldrup, B.N. Singh, and M. Victoria. To be published in Journal of Physics F: Metal Physics.

PAPER II: 'Positronium-like positron states in He bubbles in 600 MeV proton irradiated Al.', Kjeld O. Jensen, M. Eldrup, B.N. Singh, S. Linderoth, and M.D. Bentzon. To be published in Journal of Physics F: Metal Physics.

PAPER III: 'Noble gas bubbles in metals: molecular dynamics simulations and positron states.', Kjeld O. Jensen and R.M. Nieminen. To be published in Physical Review B.

1. INTRODUCTION

The positron annihilation technique (PAT) has in recent years found increasing use in a wide range of investigations of condensed matter, see e.g. refs. 1, 2, 3, 4, and 5. In studies of metals the sensitivity of PAT to defects such as vacancies, vacancy clusters, voids, and (possibly) dislocations has been especially useful. The main subject of the present thesis is the application of the positron annihilation method to investigations of a particular type of defect, namely precipitates of noble gases, conventionally called gas bubbles, in metals [6]. Such defects are formed whenever noble gases are introduced in metals, e.g., in future fusion reactor materials where He will be produced by neutrons escaping from the fusion plasma, and may have strong deleterious effects on the materials properties [7]. The primary objective has been to determine the state of a positron trapped in a bubble and how the gas inside the bubble influences the measurable positron-electron annihilation characteristics. This has been done by a combination of experimental and theoretical work, where the predictions of the theory was compared to the experimental results and applied in the interpretation of these results.

A detailed account of the results is given in the three preprints of articles appended to the thesis (these reprints are not included in the present report), whereas the main text provides a broad introduction to the field of study and gives an overview of the results obtained.

The two chapters following this introduction are both of introductory nature. Chapter 2 deals with the positron annihilation method, while chapter 3 reviews the properties of noble gases and their precipitates in metals. The theoretical results are presented in detail in Paper III and a shorter account is found in chapter 4. Chapter 5 exposes the framework used in the interpretation of the positron results in the following chapters and shows how information about the gas bubbles in a sample can be extracted from the positron data. The main experimental results of the present work have been obtained for aluminium samples in which helium was introduced by irradiation with 600 MeV protons. The results for samples irradiated at low temperatures, which can be interpreted within the framework given in chapter 5, are presented in Paper I and chapter 6. The results for the samples irradiated at higher temperatures reveal that the positron state within the bubbles is markedly different from the one in the low-temperature samples. This makes a different approach to the interpretation and discussion of the results necessary, and they are thus presented separately in Paper II and chapter 8. In addition to

the Al-He results the present work also included experimental measurements on copper and nickel samples incorporating a high concentration of krypton. No detailed presentation in the form of a paper is given of these results but a short account is included in chapter 7 mainly to provide a background for the theoretical results for the Cu-Kr system (Paper III and chapter 4). Chapter 9 provides a broad summary of the major results and chapter 10 concludes the thesis.

2. THE POSITRON ANNIHILATION TECHNIQUE.

In the following a short introduction to the field of positron annihilation studies of materials is given. More general and extensive reviews can be found in the book written by West [1], in the books edited by Hautojärvi [2] and by Brandt and Dupasquier [3] as well as in the proceedings from the latest international conferences on positron annihilation [4,5].

2.1 Basic principles.

The basic process underlying all positron studies of matter is the annihilation of an electron with its anti-particle, the positron, resulting in the emission of (in most cases two, see below) gamma-rays. A typical positron annihilation experiment consists of introduction of positrons into the sample material and detection of the resulting gamma-quanta by nuclear detection techniques. The source of positrons in such an experiment is normally a beta-emitting isotope such as ^{22}Na. The measurable properties of these gamma-quanta provide useful information about the annihilating electron-positron pair and consequently about the material in which the positrons annihilate.

The number of gamma-rays emitted in the annihilation is governed by the selection rules associated with the annihilation process due to conservation of spin and parity as well as energy and momentum [1] (the conservation of the latter two quantities excludes one-photon annihilation unless momentum is transferred to a third body; for this reason this mode of annihilation is highly unlikely [1]). For a free positron in a medium annihilation with an electron with a spin anti-parallel to that of the positron (i.e. the total spin of the two particles is 0) with the emission of two gamma-rays has the highest probability. The spin-averaged cross-section for 3-gamma annihilation (which requires the annihilating particles to be in a triplet spin state, i.e. a state with parallel spins) is only about 1/370 of the 2-gamma cross-section (anti-parallel spins) [1]. Hence for annihilation of free positrons only 2-gamma annihilation is important. When bound, spin-correlated electron-positron states such as ortho-positronium are formed 3-gamma annihilation can also be significant. However, such bound states are normally excluded in metallic systems because of the screening action of the conduction electrons (although an exception to this rule is described in chapter 8). Therefore, it will in the following be assumed that annihilation takes place with emission of two gamma-quanta. The properties of positronium and positronium-like states are discussed in chapter 8.

The conservation of energy means that the total energy of the two annihilation quanta is $2m_o c^2 \approx 2\times511$ keV (m_o is the electron mass, c the speed of light) less the sum of the potential energies of the electron and the positron in the medium (including the mutual binding energy), which normally is insignificant compared to $m_o c^2$ (and will consequently be neglected in the following). In the centre-of-mass frame of the particles the two gamma-quanta share this energy equally and they are emitted in exactly opposite directions. In the laboratory frame of reference there is a small deviation from co-linearity when the centre-of-mass momentum is non-zero. The geometry is shown in Fig.1. The angle Θ is given in terms of the momentum component p_T transverse to the direction of emission of the gamma-rays as

$$\Theta \approx p_T/m_o c \ . \qquad (2.1)$$

This equation assumes the angle Θ to be small. The distribution of angles measured experimentally (see description of the method below) normally extends up to about 15 mrad (mrad = milliradians, 1 mrad = 0.057^o). Similarly, the energies of each of the gamma-rays deviate from the energy in the centre-of-mass frame, i.e. $m_o c^2$, due to the Doppler effect. Referring to Fig.1, the energies of the two quanta is seen to be given by:

$$E_{\pm} \approx m_o c^2 \pm cp_L/2, \qquad (2.2)$$

where p_L is the longitudinal momentum along the direction of emission.

The probability of a two-photon annihilation event at a momentum $\mathbf{p}$ in a one-positron, many-electron system can be expressed as [9]

$$\Gamma(\mathbf{p}) = (\pi r_o^2 c)/(2\pi)^3 \times \int d\tau \int d\mathbf{x}\, \exp(-i\mathbf{p}\cdot\mathbf{x})\, \Psi(\mathbf{x},\mathbf{x},\tau)\,^2 . \qquad (2.3)$$

In this equation $\Psi(\mathbf{r}_+,\mathbf{r}_1,\tau)$ is the initial many-body wave function with $\mathbf{r}_+$ representing the positron coordinate, $\mathbf{r}_1$ is an electron coordinate and τ stands for the remaining electron coordinates: $\mathbf{r}_2$, $\mathbf{r}_3$, ... , $\mathbf{r}_n$. The constant r_o is the classical electron radius (equal to $e^2/m_o c^2$, e being the electron charge). In the so-called independent particle model the many-body wave function is represented by a product of a positron wave function $\Psi_+(\mathbf{r})$ and a Slater determinant of single-particle electron states $\Psi_j(\mathbf{r})$. Equation (2.3) can then be transformed into:

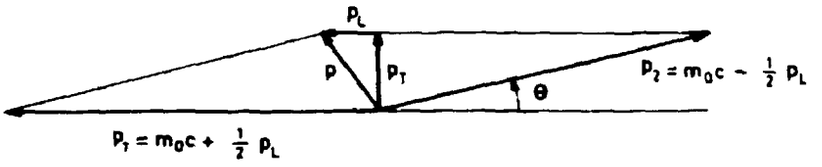

Fig.1. Vector diagram of the momentum conservation in the 2-gamma annihilation process. The momentum of the annihilating pair is denoted by **p**, subscripts L and T refer to longitudinal and transverse components, respectively. Taken from [8].

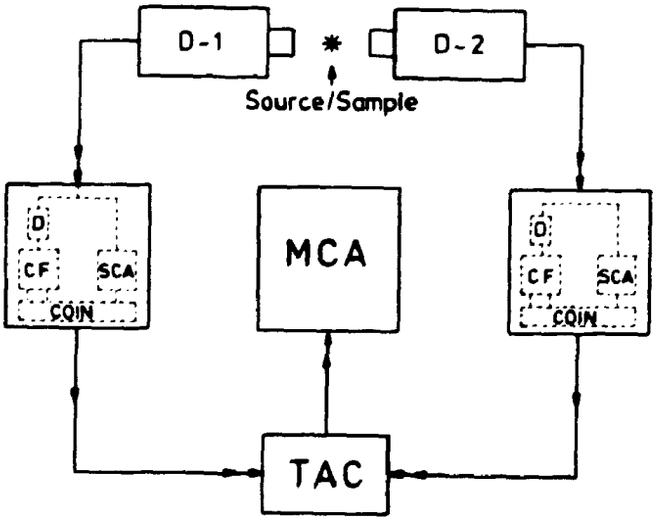

Fig.2. Schematic diagram of a lifetime spectrometer. The source is sandwiched between two samples. D-1 and D-2 are the detectors. The discriminators allow simultaneous discrimination of time and energy as indicated inside the boxes (D is a delay, CF a constant fraction pulse shaper, SCA a single channel analyser, and COIN a coincidence unit). TAC is a time-to-amplitude converter and MCA a multichannel-analyser. Taken from [12].

$$\Gamma(\mathbf{p}) = (\pi r_o^2 c)/(2\pi)^3 \times \sum_j \left| \int d\mathbf{r}\, \exp(-i\mathbf{p}\cdot\mathbf{r}) \psi^+(\mathbf{r}) \psi_j^-(\mathbf{r}) \right|^2 . \qquad (2.4)$$

From this equation it is seen that the momentum-dependent probability of annihilation with the j'th electron is proportional to the square of the modulus of the Fourier transform of the wave function product, and the total rate is obtained by summing over all occupied electron states. In many cases the positron momentum is low compared to that of the electrons. Thus, in these cases the momentum distribution, which can be deduced from a measurement of the distribution of the angle θ (cf. Eq.(2.1)) or the deviation of the energy of the annihilation quanta from $m_o c^2$ (cf. Eq.(2.2)), is essentially that of the electrons.

The total annihilation rate λ can be obtained by integrating the momentum dependent annihilation rate over all momenta. Using the expression Eq.(2.4) for $\Gamma(\mathbf{p})$ one obtains:

$$\lambda = \int d\mathbf{p}\, \Gamma(\mathbf{p}) = \pi r_o^2 c \int d\mathbf{r}\, |\psi^+(\mathbf{r})|^2 \left[\sum_j |\psi_j^-(\mathbf{r})|^2\right] . \qquad (2.5)$$

According to this formula the mean lifetime (normally just referred to as the lifetime) $\tau = \lambda^{-1}$ thus is a measure of the electron density sampled by the positron. However, the values calculated by the independent particle expression, Eq.(2.5), based on the electron densities of the system without the positron present are generally much too low, e.g., in defect-free Cs the Eq.(2.5) value is about a factor of 40 lower than the experimentally determined value. This is due to the fact that the Coulomb attraction between the positron and the electrons has been neglected in the independent particle description. This interaction leads to an enhancement of the electron density at the position of the positron, which in turn leads to a higher annihilation rate. In theoretical calculations of λ this enhancement has to be taken into account, f.ex. as it is done in the theoretical model described in chapter 4.

2.2 Experimental methods.

The experimental techniques available in positron studies include the lifetime, angular correlation, and Doppler broadening techniques. These techniques, which all probe bulk properties of the samples studied, are normally referred to as 'conventional' as opposed to the positron beam techniques to be described later, which can be used to investigate the surface and near-surface regions of solids. Reviews of the experimental positron techniques can be found in refs. 10 and 11.

The positron source most commonly used in conventional positron measurements is the radioactive isotope ^{22}Na, which has a maximum positron emission energy of 545 keV and a half-life of 2.6 years.

In lifetime measurements one exploits the fact that when the positron is emitted from a ^{22}Na nucleus there is almost simultaneous emission of a 1.28 MeV gamma-ray. The spectrometer used in lifetime experiments consists of two detectors, one detecting the 'birth' gamma-ray providing the 'start' pulse to a time-to-amplitude converter (TAC), the other detecting one of the annihilation quanta providing a 'stop' pulse for the TAC. Figure 2 shows a diagram of a typical setup. The two (identical) detectors normally consist of plastic scintillators coupled to photomultiplier tubes. The heights of the signals from the detectors allow discrimination of the signals according to the energy of the detected gamma-quantum. Figure 3 shows schematically the spectrum of signal heights recorded by one of these detectors in a positron experiment using a ^{22}Na source. The probability of photo-absorption is very low in this type of detector. Thus only Compton scattering events contribute significantly to the recorded spectrum. The Compton edge due to the 1.28 MeV gamma-ray is seen at ~1.06 MeV, and the edge due to the annihilation quanta is at ~340 keV. Indicated in Fig.3 is a typical choice of pulse height windows for the disciminators coupled to the two detectors. The upper window used for the 'start' detector selects pulses due to 'birth' gamma-rays, while the lower energy window corresponding to the 'stop' detector selects events (primarily) due to the annihilation quanta. The distribution of heights of the TAC output signal is stored by a multi-channel analyser (MCA). The TAC signal height is proportional to the time between the 'start' and 'stop' pulses. The lifetime spectrum recorded by the MCA thus consists of a histogram showing the distribution of positron lifetimes. An example of a lifetime spectrum is shown in Fig.4. The time resolution, i.e. the accuracy of the time measurement for a single event, is for a typical spectrometer characterized by a full-width-at-half-maximum (FWHM) of 200-300 ps.

In a typical lifetime experiment the samples and the source are arranged in a 'sandwich' geometry with a source made by depositing a small amount of ^{22}Na onto a thin (~1 mg/cm^2) foil which is subsequently covered by another similar foil. This source is 'sandwiched' between two identical samples thick enough to ensure that all positron emitted are stopped in the samples. The implantation profile of positrons from a ^{22}Na source is approximately exponential and the samples must have a thickness of about 0.1 g/cm^2 (~0.4 mm for Al) to insure that more than 99 % of the positrons stop inside the

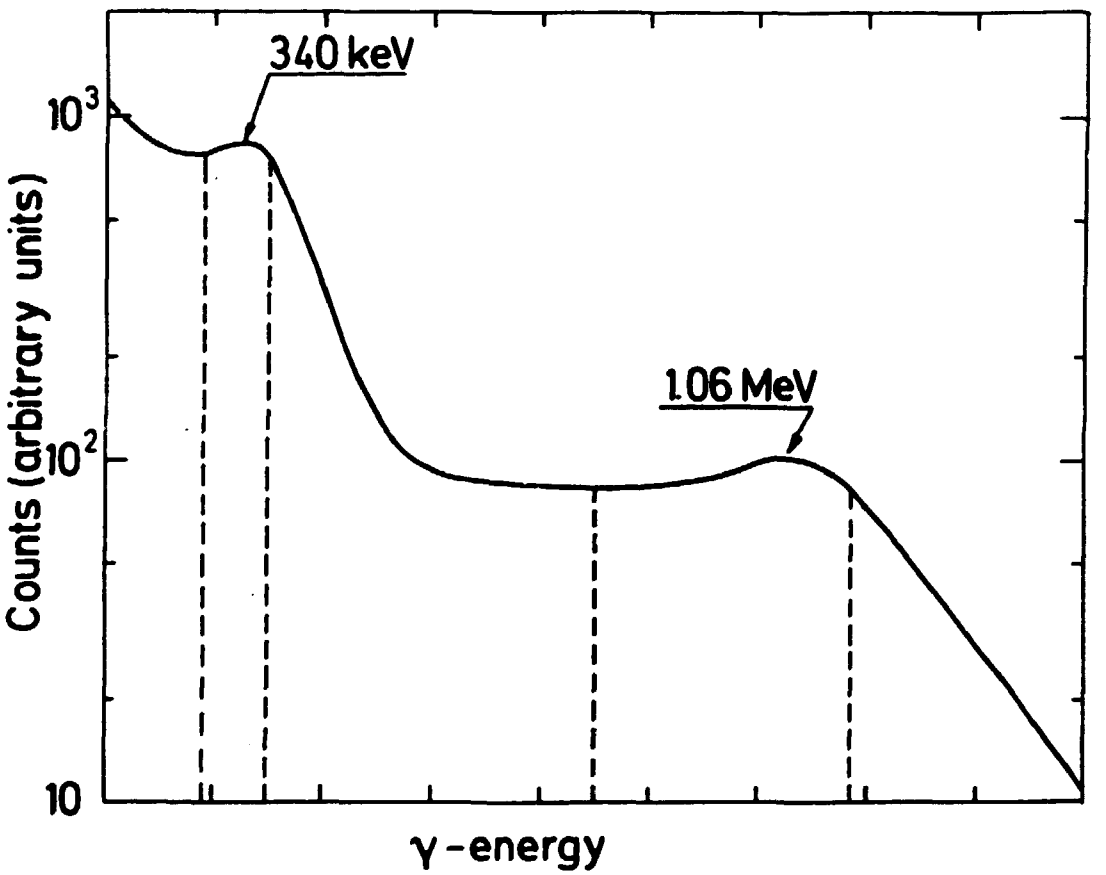

Fig.3. Spectrum of events measured by one of the detectors in a positron lifetime setup in an experiment with a ^{22}Na source (schematic). Typical settings for the windows of the single channel analysers are shown by the broken lines. The energies indicated correspond to the Compton edges for the 511 keV and 1.28 MeV gamma rays. From [13].

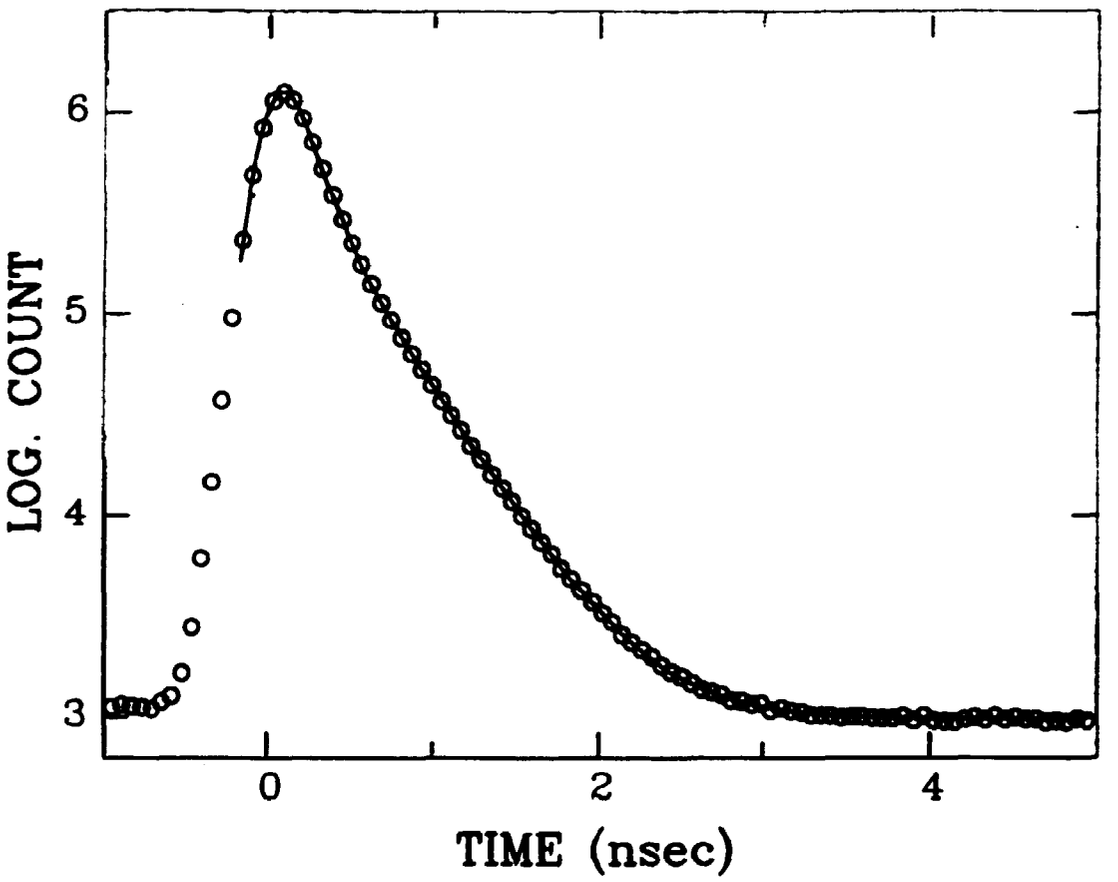

Fig.4. Example of a measured lifetime spectrum. The full curve has been fitted to the measured points according to Eq.(2.6) with two decaying exponentials each of 50 % intensity: one corresponding to the lifetime of positrons in the sample under study (proton-irradiated Al, cf. chapter 6) of lifetime 347 ps and one with a lifetime of 112 ps corresponding to positrons annihilating in the Cu discs surrounding the sample. The presence of two separate components can clearly be seen by the change of slope at the right-hand side of the curve. The spectrometer time resolution is about 250 ps FWHM.

samples [14]. In most of the experiments performed in the present work the sample-source arrangement was not the usual 'sandwich', however. The ^{22}Na was produced by nuclear reactions during irradiation with 600 MeV protons of the Al samples and the positron source was thus internal. Hence, only a single sample was required in each measurement (see chapter 6 for further details). Typical source strengths for lifetime experiments are in the range 10-100 μCi (0.4-4 MBq). These source strenghts imply that the average time between emission of positrons is of the order of 1 μs, which is substantially longer that the positron lifetimes in metals of less than 1 ns. Thus usually only a single positron is present in the samples at a time. This insures that the random background due to uncorrelated coincidences is kept low while the data collection rate is still acceptable. The background is seen as a constant base level in the spectrum of Fig.4.

After a lifetime spectrum has been recorded it is usually analyzed with a computer fitting procedure. If all positrons annihilate from the same state the resulting lifetime spectrum consists of just a single decaying exponential convoluted with the time resolution function of the spectrometer plus a constant background level. In general, when different positron states exist, the lifetime spectrum, N(t), contains more than a single decay component:

$$N(t) = [\sum_i A_i \exp(-\lambda_i t)] * P(t) + B \ . \qquad (2.6)$$

The function P(t) denotes the time resolution function of the spectrometer, which is convoluted with the ideal spectrum. The parameter B represents the background. The values of the parameters λ_i and A_i (the latter normally represented by the intensity $I_i = (A_i/\lambda_i)/\sum_i(A_i/\lambda_i)$) can be extracted from a measured spectrum by a least-squares fitting analysis, e.g.,with the POSITRONFIT program [15]. The results presented in the positron literature is normally given in terms of these parameters. 'Raw' lifetime spectra are very rarely published. In order to extract maximum information from the spectra the resolution function P(t) has to be well-defined and stable. The resolution function can be determined by a fitting procedure (f.ex. with the program RESOLUTION [15]) from lifetime spectra with a known (preferably simple) shape where a number of parameters defining the shape of the resolution function (normaily represented by a sum of up to three Gaussians) is determined by the least-squares fitting.

In analyses of lifetime spectra it is usually necessary to make corrections for positrons annihilating outside the samples under

study, e.g. in the positron source or in material surrounding the samples in cases where the samples are too thin to stop all positrons.

The number of separate components in a measured spectrum is not necessarily obvious. The number of components to include in the fitting analysis is therefore an important parameter. Justification of the choice of a certain number can in many cases be obtained from previous knowledge about the samples, from the consistency of the obtained results, and from the goodness of the fit. For metallic samples, where the lifetimes of individual components usually are in the range 100-500 ps, the maximum number of separate components which can be resolved is normally three.

It should be mentioned that the shape of the lifetime spectrum is not necessarily given by Eq.(2.6), since non-exponential decay components may be present. The sensitivity of the fitting analysis is normally not high enough to detect such deviations from Eq.(2.6), since the spectrum within the counting statistics can be well approximated by Eq.(2.6) if a sufficient number of exponential decay components is included in the analysis. However, in some cases, e.g., when the results can be interpreted in terms of the trapping model (see chapter 5), the spectrum is predicted to be given by Eq.(2.6).

Figure 5 shows schematically the conventional angular correlation (AC, referred to also as ACAR - angular correlation of annihilation radiation) apparatus. The positron source (typically of a strength of 1-50 mCi, i.e. considerably stronger than sources for lifetime experiments) is placed some distance above the sample (~1 cm). The directions of the two annihilation photons are defined by collimators which are narrow slits in lead blocks. The slits closest to the detectors are long slits perpendicular to the plane of the drawing, and the detectors are long scintillation crystals mounted just behind the slits, each of them coupled to one or more photomultiplier tubes. One of the detectors (including the collimator) is fixed, while the other can move to cover a range of angles θ . By varying θ it is possible to measure the number of coincidences between the two gamma-rays within a given time interval as a function of the angle between the gamma-rays. The resulting distribution of angles between the annihilation quanta is called an angular correlation curve. The apparatus shown in Fig.5 is a so-called one-dimensional AC machine, since it only measures the angle and thus the momentum of the annihilating particle pair, cf. Eq.(2.1), in one direction while integrating over the two other directions, i.e. the measured distribution is

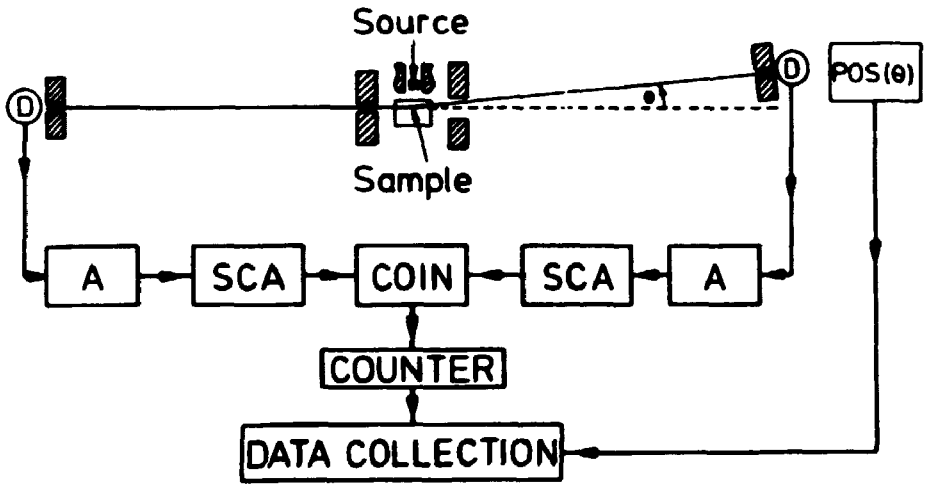

Fig.5. Diagram of a (one-dimensional) angular correlation setup. The source is external to the sample. D represents a long scintillation detector perpendicular to the drawing, A an amplifier, SCA a single channel analyser, and COIN a coincidence unit. The rectangular hatched areas are lead collimators in the form of long slits perpendicular to the plane of the drawing. From [12].

$$\Gamma_{1D}(p_z) = \int dp_x dp_y \, \Gamma(\mathbf{p}) \qquad (2.7)$$

where $\mathbf{p} = (p_x, p_y, p_z)$. All AC measurements in the present work have been performed with this type of setup. Recently a number of AC machines which measure two-dimensional AC curves, i.e. record the angular deviation between the photons in two directions simultaneously while integrating over only one direction, have been constructed [9].

The interpretation of angular correlation curves can be assisted by analyses similar to the ones used for lifetime spectra, i.e. by fitting a curve to the measured points. This analysis is, however, in many cases complicated by the fact that the functional forms of the AC curves are not known. In the present work the program PARAFIT [15] has been applied. This program allows curves to be fitted to a sum of Gaussians and inverted parabolas (each convoluted with a Gaussian). The motivation for this choice of the parametric description will appear from the discussion of AC curves for metals below.

The Doppler broadening of the annihilation line (see above) can be measured with a high-resolution solid state gamma-ray detector. The information contained in the measured energy spectra is equivalent to that obtained from AC measurements, but the corresponding momentum resolution is poorer in Doppler broadening measurements. The Doppler broadening technique has not been used in the present work.

A common feature of all the techniques described above is that they are essentially non-destructive, at least for metallic systems, in which the positrons and gamma-rays produce negligible radiation damage.

2.3 Positrons in metals.

When a positron from a ^{22}Na source is injected into a metal it is slowed down to thermal energies in a time of the order of 10 ps [16]. The initial slowing down to energies of the order of 1 eV takes place by electronic exitations in the metal, while the final stages of thermalisation takes place through interaction with phonons. Since this thermalisation time is considerably shorter than the lifetime of the positron (>100 ps), this means that most of the annihilations takes places after thermalisation of the positron. This has been confirmed experimentally by the fact that the influence of the positron momentum on the angular correlation curves of simple metals is consistent with a thermal positron momentum distribution for temperatures down to about 30 K [17]. Thus the positron momentum is generally low compared to the momenta of the electrons.

The bulk state of a thermalised positron in a defect-free metal can be described as a delocalised Bloch state. The wave function is fairly uniform throughout the unit cell with 'holes' around the positive ion cores. However, this does not imply that the true positron state is spread uniformly over the sample volume [18]. Experimental results for positrons implanted close to the surface of materials [19] and trapping of positrons into large cavities [20] (see also chapter 5) can be interpreted in terms of diffusional motion of the positron in a basically classical picture. Both theory and experiment indicate that the value of the corresponding diffusion constant is of the order of 1 cm^2/s, implying a diffusion lenght within the positron lifetime of the order of 1000 A [18].

Typical lifetimes in defect-free metals are in the range 100-200 ps with only a weak temperature variation. As noted in section 2.1, the positron-electron attraction leads to an enhancement of the electron density around the positron. In metals this enhancement takes the shape of a screening cloud of conduction electrons. The positron-electron correlation gives rise to a negative (attractive) contribution to the effective potential for the positron counteracting the static Coulomb repulsion in the ion core regions.

In simple, i.e. nearly-free-electron-like metals, most of the intensity in the (1-D) angular correlation curves is taken up by a component with a shape represented approximately by an inverted parabola. Figure 6 shows a curve measured for well-annealed, nominally defect-free Al, where the parabolic component can be seen clearly. The parabolic shape can be explained by evaluating the independent particle expression for the AC curve, Eq.(2.4), with a set of free electron wave functions, i.e. plane waves with energies up to the Fermi energy level. The cut-off angle of the parabola is determined by the Fermi momentum and is thus referred to as the Fermi angle. The near-parabolic component in simple-metal AC curves is thus due to annihilations with the conduction electrons. Because of the angular resolution of the spectrometer and the non-zero positron momentum the parbolic shape is smeared slightly, which can be represented by convoluting the parabola with a Gaussian. In addition to the conduction electron component there is also a contribution due to annihilations with more tightly bound core electrons with a shape which usually can be approximated well by a Gaussian. This component is broader than the conduction electron component due to the higher momenta of the core electrons as can be seen in the example of Fig.6. In metals with more complicated electron structures more structure can be observed in the AC curves, especially in two-dimensional AC

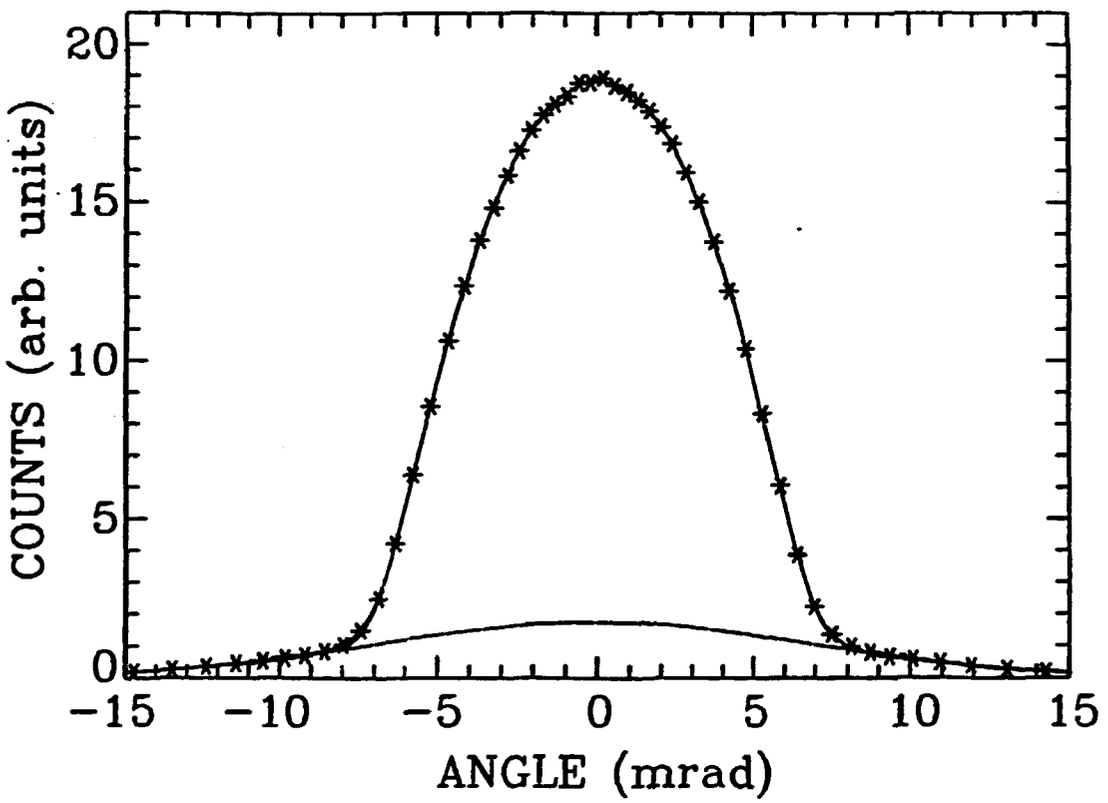

Fig.6. Angular correlation curve measured for well-annealed Al (O.E. Mogensen, unpublished). The full curve has been fitted to the measured points. It consists of a Gaussian component also shown separately as the broken curve and a component with the shape of a parabola convoluted with a (narrow) Gaussian. The angular resolution is about 1 mrad.

measurements, which has proven to be a useful tool in the study of Fermi surfaces of metals and alloys [9]. However, in 1-D AC curves, which have less sensitivity to these details, the main features still resemble those described above, i.e. an approximately parabolic component due to the conduction electrons and a broader core electron contribution.

Due to the strong repulsion between a positive ion core and a positron any region with lower than average ion density such as vacancies and vacancy clusters attracts the positron and thus forms a possible trapping site for the positron. Trapped in such a defect the positron will experience a lower electron density than in the defect-free bulk of the metal and its lifetime is therefore increased. Similarly, the AC curve becomes narrower both because the average conduction electron density sampled by the positron is lower, thus reducing the Fermi angle of the parabolic component, and because the fraction of annihilations with the high momentum core electrons is reduced. These changes in the annihilation characteristics for defect-trapped positrons forms the basis of the now well-established use of positron annihilation in metal defect studies.

The annihilation characteristics depend on the type of defect in which the positron is trapped. This makes it possible to a certain extent to differentiate between the different defects. Further, the rate at which positrons are trapped (see chapter 5) contains information about the concentration of defects.

Since most of the measurements in the present work have been performed on aluminium samples, the variation of lifetimes associated with different defect states of the positron will be illustrated with Al as a specific example. The relative change in lifetimes found for other metals are generally similar. In Al the positron lifetime in defect-free bulk is about 164 ps. When the positron is trapped in a vacancy the lifetime increases to about 250 ps. This lifetime can easily be distinguished from the bulk lifetime experimentally. The vacancy concentration, C_v, required to produce a measurable change in the lifetime spectra is about 10^{-6} (1 ppm). When C_v is larger than about 100 ppm very nearly all positrons are trapped before annihilation.

The lifetime of the trapped positron component observed when dislocations are introduced in Al is approximately the same as the vacancy lifetime. The exact nature of the positron trap associated with dislocations is still a matter of debate [21]. The positron is probably not trapped by the dislocation line itself but rather in more open-volume defects such as jogs associated with the dislocation (see

further discussion in Papers I and II).

When vacancies are agglomerated in clusters trapped positron lifetimes larger than the single-vacancy lifetime are observed. For small vacancy clusters the lifetime generally increases with the cluster size [22]. In vacancies and small clusters the positron wave function extends over the whole defect volume. However, as the cluster size increases above a size estimated to be around 5-10 A radius [23], the positron wave function will be localized at the surface of the cavity due to the image force between the positron and the metal electrons and the lifetime will be fairly insensitive to the cluster size at a value of about 500 ps.

The primary objective of the present work has been to investigate to what extent a positron trapped in a cavity is affected by a content of gas atoms such as He in the cavity. In particular the effect on the positron lifetime has been investigated. The conclusion which will appear from the following is that the lifetime indeed depends on the density of gas inside the cavity. Similarly, the shape of the AC curve also depends on the gas content.

2.4 Positron-surface interactions.

A new development in the field of positron physics in recent years has been the possibility to study positron-surface interactions using variable energy positron beams (recent reviews are provided by Mills [19] and by Dupasquier and Zecca [24]). The construction of variable energy positron beams relies on the fact that when positrons with a wide distribution of energies, e.g., from a radioactive source are injected into a material there is a certain chance that the positron will be re-emitted after thermalisation with an energy of the order of 1 eV. This process relies on the fact that the positron work function of several materials is negative, i.e. the positron gains energy as it leaves the material [19]. In a positron beam setup the crystal in which the slowing down and re-emission process takes place is referred to as the moderator and the process itself as moderation. Further handling and transportation of the positrons emitted from the moderator can be done by electrostatic and magnetic fields. The low energy-spread of the moderated positrons means that a well-defined beam of positrons can be obtained, which can be accelerated and guided towards a target sample.

The range of the positron in the sample depends on the injection energy. It is thus possible to probe different depths by varying the positron energy. For implantation with energies of the order of 5 keV

the ranges are of the order of 1000 A [19]. This is comparable to the length of diffusion before annihilation of a non-trapped positron in a metal [18]. After the positron has slowed down it can undergo different processes. It may annihilate while diffusing in the solid or get trapped in a defect with subsequent annihilation from the trapped state. It may also reach the surface, where it can be ejected either as a free positron or bound to an electron in a positronium atom, or the positron can get trapped in a surface state [19]. The measurable properties in positron beam experiments include the branching ratios between the different channels available for the positron at the surface [19], the energies [25, 26, 27, 28] and emission directions [25, 29] of the particles emitted from the surface as well as the annihilation characteristics such as the lifetime [30] and the AC curve [27, 28] of positrons in the surface state. This surface state is presumably equivalent to the one found in large cavities (see above), and the interactions between positrons and external surfaces are presumably similar to those taking place in cavities, i.e. at internal surfaces. The results from the positron beam experiments can therefore be used in the interpretation of (conventional) positron experiments on cavity-containing samples. Thus, although the present work does not include any positron beam experiments, reference to variable energy positron results will frequently be made. The positron surface state will be discussed further in chapter 4.

3. NOBLE GASES IN METALS.

The present chapter provides a brief description of some of the properties of noble gases in metals and the methods which can be used to characterize the defects created when noble gas atoms are introduced into a metallic matrix. Most of the discussion is dealing specificly with helium but the general properties described applies for all the noble gases.

3.1. He bubbles. Properties and experimental methods.

The generation of He during irradiation in metals is known to have strong deleterious influence on materials properties [7]. This kind of situation will be encountered particularly in future fusion reactors since the 14 MeV neutrons escaping the fusion plasma will produce He by (n,α) reactions in the surrounding reactor walls. Accordingly, there has been a growing interest in the problem of He and He-defect interactions in metals, not only from a technological point of view [7] but also in terms of achieving a better fundamental understanding of the behaviour of He in metals [6].

The key property that governs the behaviour of He in metals is its extremely low solubility. This means that when He atoms are introduced into a metal they have a strong tendency to precipitate. Initially when the He concentration is still low small He-vacancy complexes (clusters) are formed, which gradually as the amount of He increases grow into larger He filled cavities conventionally called He bubbles. For sufficiently high He concentrations this eventually leads to detrimental effects on the mechanical properties of the metal [7]. These effects are generally attributed to He bubbles at grain boundaries [7].

It is thus important to develop techniques for the characterisation of He bubbles. The most direct determination of bubbles sizes and concentrations can be obtained by transmission electron microscopy (TEM). However, TEM is sensitive only to bubbles with radii larger than about 10 A. Further, TEM normally provides no direct information on the amount of gas inside the bubbles. A number of complementary techniques have been applied in an attempt to determine He densities inside bubbles [31], among these positron annihilation. Other techniques include electron energy-loss spectroscopy (EELS) and vacuum ultra-violet absorption spectroscopy (VUVAS). Both these methods monitor the variation of the 1S-2P transition energy ΔE in the He atom with He density n_{He}. Theoretical calculations predict a relation between n_{He} and ΔE given approximately by $\Delta E = K \times n_{He}$, where K is a

proportionality constant. There is, however, some controversy as to the value of K [31]. This point is further discussed in chapter 9 and in Paper I.

The densities of He inside bubbles estimated by various methods are generally very high [31], e.g. in bubbles of 10 A radius in Al n_{He} values of about 10^{29} m^{-3} have been found. This density is much higher than the density of liquid He at ambient pressures of about 2×10^{28} m^{-3}. The high compression of the He implies very high pressures inside the bubbles. The He equation-of-state (EOS) [31] implies that a density of 10^{29} m^{-3} corresponds to a pressure over 2 GPa, i.e. over 20000 atm. The ideal gas EOS is highly inappropriate at these densities.

The fact that such high densities can develop in the bubbles is a manifestation of the insolubility of the He in the metal, since the He pressure has to be very high to make it energetically favourable for a He atom inside a bubble to go into solution in the metallic matrix. However, it is normally not re-solution of He into the metal which limits the amount of He that can be contained within a cavity of a certain size but rather the limited shear strength of the metal. If the pressure inside a bubble reaches above a certain limit it will be energetically favourable for the bubble to increase its volume by punching out an interstitial dislocation loop. For very small bubbles emission of single self-interstitials from the bubble may also take place. The limiting pressure p_L for loop-punching to occur can in a simple model be expressed as [32]

$$p_L = 2\gamma/r + \mu b/r, \qquad (3.1)$$

where r is the bubble radius, γ is the specific surface energy of the metal, b is the length of the dislocation Burgess vector, and μ is shear modulus of the metal.

If the temperature is sufficiently high, absorption of thermal vacancies will be able to relax the pressure inside the bubbles to an equilibrium value determined by the balance between the pressure of the gas, which tends to expand the bubble, and the surface tension, which favors reduction of the bubble surface area. For bubbles where this balance has been achieved, normally referred to as equilibrium bubbles, the pressure p_{eq} can in a simple model be expressed as [32]

$$p_{eq} = 2\gamma/r \ . \qquad (3.2)$$

Thus, according to Eq.(3.2) the pressure is a unique function of the

bubble radius for equilibrium bubbles. This relation implies that when it is reasonable to assume the bubbles in a sample to be in equilibrium, it is possible to estimate the pressure inside the bubbles from bubble radii determined e.g. by TEM. Similarly, the bubble radius can be estimated if a determination of n_{He} has been made.

Note that both relations Eqs.(3.1) and (3.2) imply that small bubble sizes in general correspond to high pressures (and thus high gas densities) inside the bubbles.

It was indicated above that bubbles are formed and gradually increase their size when He atoms are introduced into a metal. However, even when no further He is introduced, the bubbles can grow during annealing of the samples. The increase in bubble size is then normally accompanied by a reduction in bubble concentration. The basic mechanism underlying this coarsening of the bubble population during annealing is still a matter of debate [33,34]. There are two distinct processes which can lead to bubble growth. One involves the migration and subsequent coalescence of bubbles [35,36]. Bubble migration can, e.g., take place by diffusion of individual atoms on the bubble surface. The other is a ripening process involving solution and re-absorption of He atoms [37]. At the same time as these processes take place, bubbles interact with thermal vacancies, which at high temperatures presumably maintain the bubbles at thermal equilibrium. Since bubble radii increase this means that the pressure and hence the He density inside the bubbles decrease during annealing, cf. Eq.(3.2). If the concentration of thermal vacancies is low the bubbles may also increase their volume by the loop-punching mechanism. In the present work a number of annealing experiments have been performed in which bubble growth has been followed by positron lifetime measurements. However, it has not been possible to assess which of the above-mentioned processes is responsible for the observed annealing behaviour of the bubbles.

3.2. Positron annihilation studies of He bubbles in metals.

The first study of a He-injected metal by positron annihilation was made by Snead et al. [38]. Al samples in which He was implanted with 50 MeV He ions from a cyclotron to a total He concentration of 0.6 ppm were studied by the positron lifetime technique. Samples were studied both as-prepared and following isochronal annealing. Although the lifetime of the defect component resolved in the lifetime spectra initially was about 250 ps, the value characteristic for mono-vacancies or dislocations, annealing resulted in a defect lifetime

rising above this value up to about 310 ps. This indicated that positrons were trapped in defects larger than mono-vacancies, presumably He bubbles. No consideration of the influence of the He atoms on the lifetime of the trapped positrons were made.

In later studies the amount of He injected into the samples has generally been higher than in this first study, typically of the order of 100-1000 ppm. In a positron lifetime study of Al implanted with 27 MeV He Hansen et al.[39] investigated the possibility of extracting quantitative information about the He bubbles from the positron data. Special attention was devoted to the question of relating the measured lifetime for the trapped positrons (which increased from the initial 360 ps up to 450 ps as the annealing temperature was increased) to the He density inside the bubbles. Based on positron lifetime results for bulk (fluid) He semi-quantitative density estimates were obtained consistent with the range of densities estimated by other methods (see above). Using this density information as well as the trapping rates of positrons into the bubbles estimates of bubble radii and concentrations were made. However, insufficient knowledge of the positron state inside bubbles and hence the relationship between the positron lifetime and the He density precluded a truly quantitative analysis of the data. Also, the use of trapping rate information in the derivation of bubble parameters lacked a firm basis because the relation between the size of the bubbles and the trapping rate per bubble (the specific trapping rate, see chapter 5) had not been assessed experimentally.

Other workers [40-42] have performed positron studies of He bubbles, where questions similar to those mentioned above were addressed, although generally in less detail.

Parts of the work to be described in the following chapters can be viewed as an extension of the investigation of Hansen et al. described above. One of the major aims has been to establish the relationship between positron lifetime and He density inside bubbles and to demonstrate that bubble parameters can be estimated reliably from positron annihilation results.

4. POSITRON ANNIHILATION IN GAS BUBBLES. THEORY.

4.1. Introduction.

It was noted in the end of the previous chapter that the idea of relating the lifetime of positrons trapped in gas bubbles to the gas density inside bubbles has been considered by previous workers. However, only semi-quantitative density information could be obtained because no detailed account of the positron behaviour in the bubbles was made, and the proposed relationships between positron lifetime and gas density therefore lacked a firm basis. The primary purpose of the theoretical part of the present work has been to provide a foundation for the interpretation of the PAT results and to derive relations between positron lifetime and gas density for a selection of metal-noble gas systems.

The results demonstrate that in large bubbles (radii above ~10 A) the positron is trapped at the bubble surface, i.e. at the gas-metal interface. To determine the positron characteristics it is necessary to know the atomic arrangement close to the interface. This information has been obtained by sets of molecular dynamics (MD) simulations for Al-He and Cu-Kr interfaces. The MD method has earlier been applied to He-filled platelets [43] and small He-vacancy clusters [44], but no metal-noble gas interface results have been published previously.

Calculations for positrons trapped in small vacancy-gas clusters are also presented, supplementing the interface results applicable only to large bubbles.

A short account of the calculations for the Al-He system has been published previously [45].

4.2. Molecular dynamics simulations.

In general, large gas bubbles (radii larger than a few tens of A) have three-dimensional faceted shapes. The problem of describing the atomic structure at the bubble surface can therefore be approached by considering a planar metal-noble gas interface representing the facets.

Briefly, the molecular dynamics method [46] employed in this study consists of solving the classical equations of motion numerically for a set of particles (typically of the order of 1000) confined within a computational cell. The forces acting between the particles are

calculated from pair-potentials defined for each type of particle pairs. The simulation proceeds in a series of time-steps, where the changes in particle positions and velocities at each step are determined by forces calculated based on the positions at previous steps. The time between each step has in this work been chosen as 5×10^{-15} s. The boundary conditions on the faces of the cell were chosen to be periodic, i.e. the unit cell is assumed to be repeated infinitely in all three spatial dimensions. At the outset of the simulation the particles are placed in a geometry according to the system which is to be simulated and each particle is give a random velocity corresponding to the simulation temperature. As the simulation proceeds the particle velocities are scaled at frequent intervals to keep the temperature at a constant value. After a while the temperature has been equilibrated, so that no further velocity corrections are required, and various properties of the system such as the time-averaged density profiles can be evaluated.

For the Al-He system a sandwich geometry was applied with 6 layers of Al atoms ((001) planes) containing in total 192 atoms separating two sets of up to 300 He atoms in a box of constant volume with periodic boundary conditions in all three dimensions. The He atoms were initially arranged in a regular array. However, any information about the initial He positions was rapidly lost as the simulation proceeded.

Three separate interaction potentials had to be defined, one for each type of particle pairs: Al-Al, He-He, and Al-He. Details of the potentials can be found in Paper III.

The simulations were run for up to 1200 timesteps of 5×10^{-15} s. First the system was equilibrated to the temperature required, this being 300 K in most cases. Thereafter the time-averaged density profile $n_{He}(z)$ perpendicular to the interface was calculated using z-bins of 0.1 A (i.e. the z-axis was divided into intervals of length 0.1 A and the He atoms were grouped according to the interval they belonged to). The two sides of the 'sandwich' were combined into one profile. Two examples of profiles are shown in Fig.7. With increasing mean He density $\bar{n}_{He}$, defined as the average value for large z, a strong peak in the He density profile first develops near the Al surface and secondary peaks in the fluid follow. The surface peak is not associated with the physisorption well in the He-Al interaction (it appears also when no attractive part is included in the He-Al potential). Rather it originates from the statistical packing of atoms next to the repulsive metal surface, much as with hard spheres near an impenetrable wall [47].

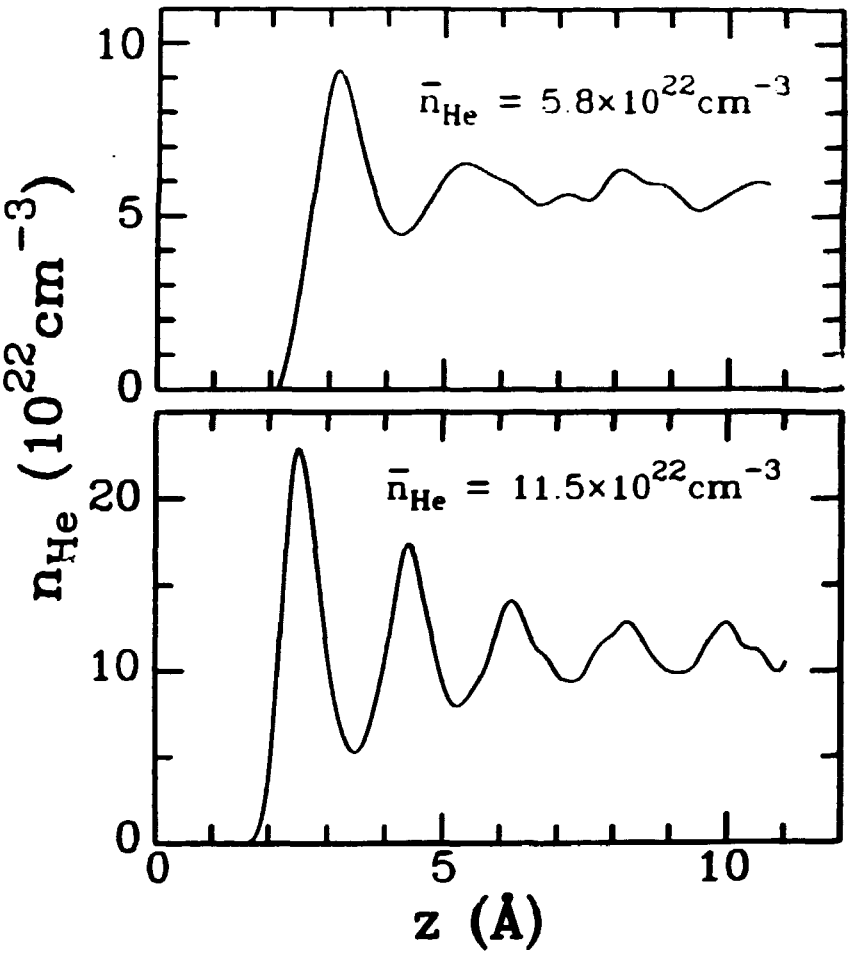

Fig.7. One-dimensional He density profiles perpendicular to the Al(001) surface obtained by molecular dynamics simulations. The outermost Al layer is at z = 0. The mean He densities, $\bar{n}_{He}$, indicated are the average values for large z. The simulation temperature was in both a) and b) 300 K. The profiles have been averaged over 500 timesteps (2.5 ps) after equilibrium was attained.

No appreciable enhancement of the lateral ordering (i.e. parallel to the interface) is observed in the He layer closest to the interface compared to the deeper layers representing the bulk structure. Lateral corrugations of the distributions of He atoms near the metal are only detectable at the highest densities and are in all cases weak.

4.3. Positron surface state calculations.

For large, empty voids in aluminium the lowest-energy positron state is the surface state [48]. This state can be modeled as an image-potential induced state [49], where the positron is trapped in the potential well induced by the image force between the positron in the vacuum and the metal. The recent, alternative 'physisorbed Ps' model [50] of the surface state will be discussed briefly below. From the present calculations (see below) it has been found that the surface (interface) state remains the most stable also in He-containing cavities (bubbles) for all values of the He density inside the bubble.

The positron calculations are based on an extension of the corru-gated mirror model of Nieminen and Puska [49]. The first step of the calculations is to construct the effective potential V^+ sensed by the positron at each point of the computational unit cell. For the construction of the potential V^+_{met} at a clean metal surface space is divided into two domains. Inside and in the vicinity of the surface a local-density approximation is used [51]:

$$V^+_{local}(r) = V_{corr}(n(r)) + V_C(r) \ , \qquad (4.1)$$

where V_C is the Coulomb potential calculated by superimposing atomic charge densities and $V_{corr}(n)$ is the correlation energy of a positron in a homogeneous electron gas of density n. The electron density n(r) is taken as a superposition of atomic electron densities. Outside the surface the potential is the classical image potential:

$$V_{im}(r) = -e/4(z-z_o), \qquad (4.2)$$

which in the present model is modified slightly to make the potential contours follow the contours of the electron density. In Eq.(4.2) z is the distance from the surface layer of atoms (z>0 is the vacuum side of the surface), z_o is the position of the image plane, and e is the electron charge. At each point of the unit cell outside the surface, the positron potential V^+_{met} is taken as the <u>larger</u> of the two potentials V^+_{local} and V_{im} defined by Eqs.(4.1) and (4.2), respectively. This construction mimics the continuous transition from

the local screening of the positron inside the metal to the non-local image interaction far from the surface. The constant z_o has been chosen to be 1.76 A. This value, which is close to that estimated from jellium calculations [52], reproduces well the observed binding energies to clean Al surfaces [19]. The potential at He covered surfaces is taken as a sum of metal and He contributions:

$$V^+(r) = V^+_{met}(r) + \sum_R V^+_{He}(r-R) \ , \qquad (4.3)$$

where R denotes summation over the gas atom positions. Because of the inertness and low polarisability of He, the metal-positron interaction is only negligibly affected by the presence of He atoms close to the surface and is well approximated by the positron potential at a clean metal surface calculated as described above. For positron-surface distances z larger than 2 A only the long-range image interaction survives in V^+_{met}. Thus the model assumes the positron screening charge to reside at the metal surface and there is no accumulation of electrons around the positron for z>2A. Since the MD simulations have shown that the He atoms very rarely get closer than this to the surface, this also means that the metal electrons only weakly screen the positron-He interactions. Therefore both the atomic Coulomb potential $V_{c,He}$ and the (long-range) polarisation potential [53] V^+_{pol} are included in V^+_{He}:

$$V^+_{He}(r) = V_{c,He}(r) + V^+_{pol}(r) \ . \qquad (4.4)$$

The latter is given by

$$V^+_{pol}(r) = \begin{cases} -\alpha/2r^4 \ , & r \geq r' \\ -\alpha/2r'^4 \ , & r < r' \end{cases} \qquad (4.5)$$

where α is the static dipole polarisability and r' an adjustable length parameter. As in calculations for bulk He, values of $\alpha = 1.383\ a_o^3$ and $r' = 1.57\ a_o$ (a_o is the Bohr radius) were used [53, 54]; these reproduce the correct positron-helium scattering length.

When the potential has been evaluated the ground state positron wave function is obtained from a numerical solution to the three-dimensional Schrödinger equation [55]. Examples of positron potentials and wave functions for clean and He covered surfaces are shown in Figs.8 and 9.

The positron and electron densities are used to calculate the positron annihilation rate λ. This rate is divided into contributions from gas

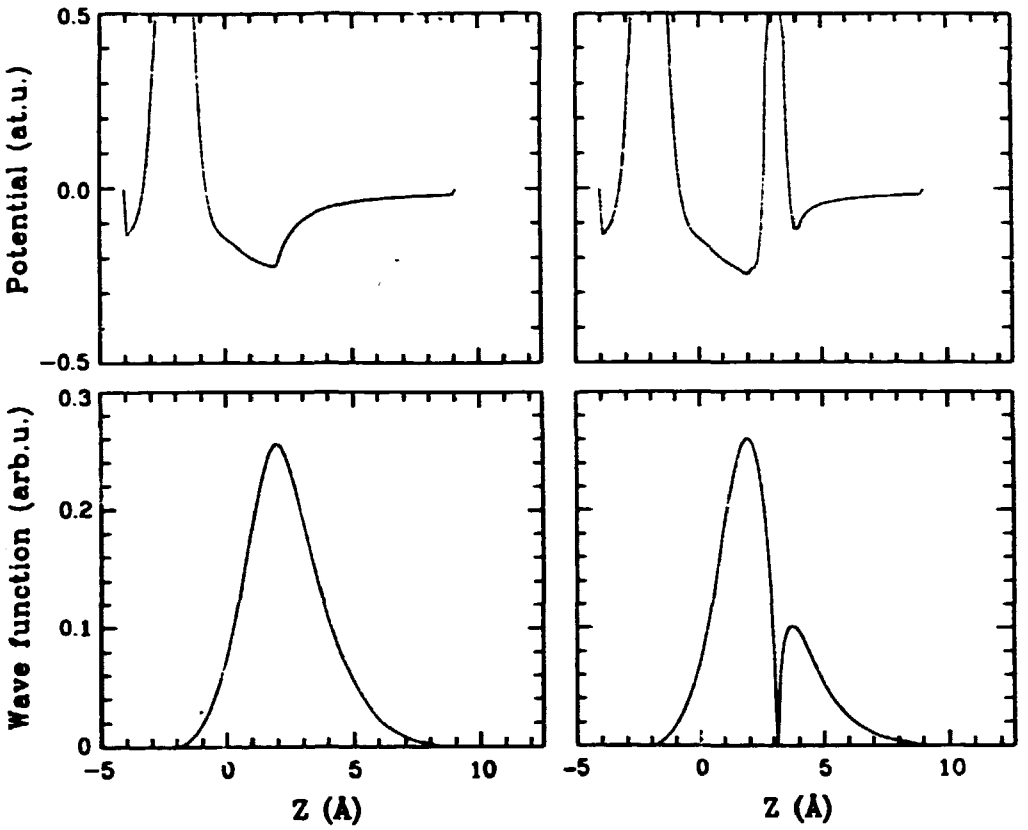

Fig.8. Potential and wave functions for a clean Al(001) surface (left panels) and Al(001) surface covered by one monolayer of He positioned at four-fold sites about 3.2 A from the Al surface (right panels). The figures show cross-sections through four-fold sites.

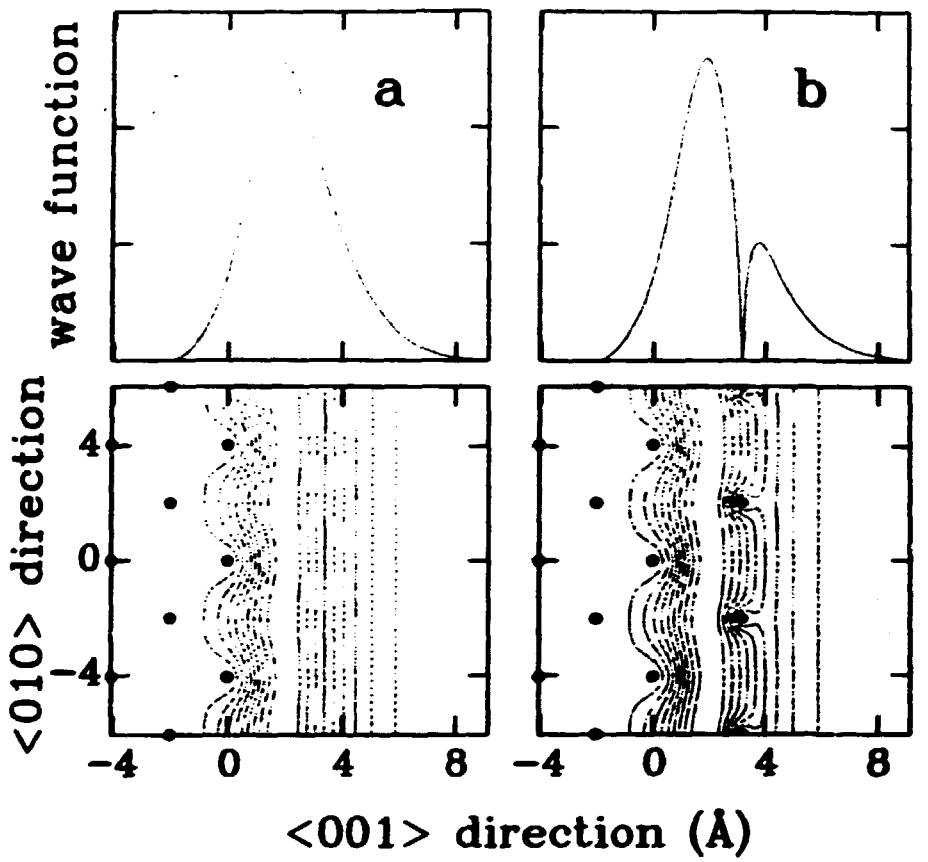

Fig.9. Positron wave functions at a) a clean Al(001) surface and b) Al(001) with one monolayer of He at four-fold sites shown as contour plots (lower panels) and cross section through a four-fold site (upper panels). The black dots denote positions of Al atoms in the plane of the paper. The He positions in b) corresponds to the dips in the wave function about 3 Å from the surface. The wave functions in a) and b) are both normalised within the unit cell and contour spacings are 1/10 of the maximum value in each case.

atom (He) electrons λ_{gas} and metal (Al) electrons λ_{met}:

$$\lambda = \lambda_{met} + \lambda_{gas}. \qquad (4.6)$$

Both rates are proportional to the overlap of the positron and electron densities, multiplied by an enhancement factor, which depends on the nature of the annihilating electrons. For λ_{gas} one can apply the independent particle description with a constant enhancement factor γ:

$$\lambda_{gas} = \pi r_o^2 c\gamma \int dr \; |\Psi^+(r)|^2 \; \rho(r) \qquad (4.7)$$

where Ψ^+ is the positron wave function, ρ the gas atom electron density, r_o the classical electron radius, and c the speed of light. Apart from the enhancement factor taking into account the effect of the electron-positron correlation on the annihilation rate this formula is identical to Eq.(2.5). In the case of He a value of 2.9 is applied for γ. This is the γ required to reproduce the experimental annihilation rate for bulk He [54].

Similarly, λ_{met} is the result of the positron-metal electron overlap. The approach originally used in the model [49] was to divide the annihilation rate into contributions from core and conduction electrons:

$$\lambda = \lambda_{core} + \lambda_{cond}, \qquad (4.8)$$

where the independent particle formula, Eq.(4.7) with $\gamma = 1.5$ [56] was used for the core electron contribution, λ_{core}, and the conduction electron contribution, λ_{cond}, was calculated based on electron gas data:

$$\lambda_{cond} = \int \Gamma(n(r)) \; |\Psi^+(r)|^2 dr \qquad (4.9)$$

where

$$\Gamma(n) = 2 + 134n \;, \; \Gamma \text{ in } ns^{-1} \text{ and } n \text{ in units of } a_o^{-3}, \qquad (4.10)$$

is the annihilation rate of a positron in a homogeneous electron gas of density n [57]. Note that $\Gamma(n)$ does not go to 0 as n tends to 0 but towards a finite value of 2 ns^{-1}, since the positron is surrounded by a cloud of screening electrons even at the lowest electron densities. Using this prescription the lifetime calculated for the surface state at a clean Al(001) surface is 398 ps. However, this approach contains an internal inconsistency when it is applied to the

surface state model. Throughout the range ($z > 2A$) where the positron is assumed to experience the classical image potential there is a related assumption that all the electronic screening charge is confined to the region inside the image potential plane. Thus, the positron is bare and the contribution to the annihilation rate from this region must vanish. A way of dealing with this problem [58] is to introduce a sharp cut-off in the local annihilation rate by setting it equal to zero in the region of space where the positron potential is taken to be the image potential while still using Eqs.(4.8) in the remaining part of space, where the local approximation is used for the positron potential. For Al(001) this yields a lifetime of 659 ps [58], which compares more favourably than the original estimate with the so-far only experimental determination of the lifetime of a positron trapped at an external Al surface of 580±10 ps [30]. However, although the introduction of the cut-off is physically well-motivated, it is not without a certain arbitrariness, and one would think that the local annihilation rate would drop less abruptly from the value inside and in the vicinity of the surface represented by Eq.(4.8) to the zero value far from the surface. We have not attempted to resolve this problem in the present calculations but used, as described below, an empirical approach to λ_{met}.

For all geometries considered, the calculations show that the λ_{met} value for Al can be approximated accurately by the value for a bare Al(001) surface since, only in a small volume (radius 0.5 A) around each He atom, the positron wave function deviates substantially from the wave function at the clean surface (see Figs.8 and 9). The deviation will therefore primarily be at some distance from the surface where the positron-metal electron overlap vanishes. The problem of calculating the absolute value of λ_{Al} theoretically outlined above leads us to use an empirical λ_{Al}. The most direct determination of λ_{Al} for a clean surface has been made in a positron beam experiment [30]. The value, $\lambda_{Al} = 1.72$ ns^{-1} (corresponding to the lifetime of 580 ps already mentioned above), however, deviates from the annihilation rate associated with nominally empty voids in Al, $\lambda_{Al} = 2.0$-2.2 ns^{-1} [20, 59-61]. Since continuity between positron lifetimes for bubbles with finite He density and voids with $\bar{n}_{He} = 0$ is desirable, we use $\lambda_{Al} = 2.0$ ns^{-1} to compute numerical values for the lifetime τ:

$$\tau = (\lambda_{Al} + \lambda_{He})^{-1}. \qquad (4.11)$$

Note that the actual value of λ_{Al} plays a role only at the instant where τ is calculated. Otherwise the results, notably λ_{He} and the dependence on the fluid density, are independent of the absolute value

of λ_{Al}.

Computational convenience imposes a requirement of relatively high symmetry on the positron surface (interface) calculations. Thus, geometries with irregular He positions such as those obtained from the MD simulations cannot be treated directly. Instead, the combination of MD and positron calculations will be made through an intermediate step where the positron model is applied to various configurations with ordered He overlayers.

In all calculations the metallic surface was chosen to be the (001) surface. The detailed results from the calculations for Al(001) with ordered single layers of He at coverages up to a full monolayer can be found in section IIB of Paper III. The binding energy of the positron to the surface is found to be increased by an amount of the order of 0.1 eV compared to the clean surface value of 2.84 eV (cf. Fig.4 of Paper III). By comparing λ_{He} values calculated for different geometries one finds that each He atom contributes additively to λ_{He}, i.e. the contribution of an indivual He atom depends on the atomic position but is independent of the position of other He atoms. This is related to the fact mentioned above that the He atoms only very locally perturb the positron wave function.

4.4. Positron results for the Al-He interface.

The additivity of λ_{He} noted in the previous section will permit one to calculate λ_{He} for a positron trapped at a He-Al interface without having to solve the positron Schrödinger equation for the specific geometry. The procedure is to find the contribution from each part (i.e. z-bin) of the He profile individually using the single layer results and subsequently add contributions from all parts of the profile to obtain the total λ_{He}. The corresponding positron lifetime τ can be calculated from Eq.(4.11) with $\lambda_{Al} = 2.0\ ns^{-1}$. By applying this procedure to the He profiles obtained for different densities of He at the interface, it is possible to obtain a relation between the positron lifetime and the He density at the interface, and thus, since the interface represents the facets of a He bubble, a relation between He density and positron lifetime in He bubbles. This relationship is shown in Fig.10. One observes that the lifetime depends approximately linearly on the He density and that the reduction from the clean surface lifetime of 500 ps is quite substantial in the density range expected to be found in real He bubbles (10^{28}-$10^{29}\ m^{-3}$). The line drawn i Fig.10 corresponds to a relationship:

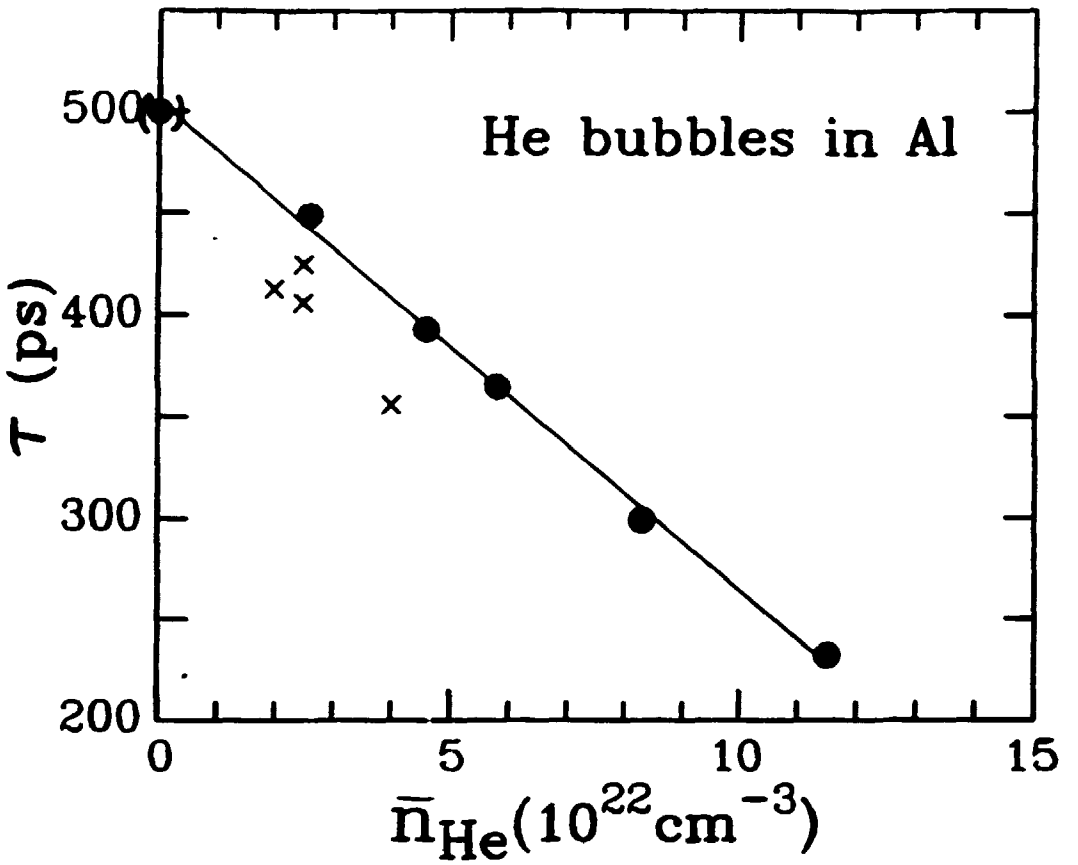

Fig.10. Lifetime for a positron trapped in a He bubble in Al vs. He density inside the bubble at 300 K. Filled circles denote theoretical interface results with $\lambda_{Al} = 2.0\ ns^{-1}$. The line is a visual fit. The crosses are based on experimental data with densities estimated by the thermal equilibrium condition.

$$\tau(ps) = 500 - 23.5 \times \bar{n}_{He}(10^{28} m^{-3}). \qquad (4.12)$$

By applying a similar additivity approach the binding energy (with respect to vacuum) of the positron to a bubble is found to increase compared to the clean surface value by up to 0.7 eV for the He densities considered here (see Fig. 8 of Paper III).

As noted all calculation have been performed for the (001) surface. However, since both the He-surface and positron-surface potentials are very similar for the low-index Al surfaces, this means little loss of generality. Similarly, one would expect that the results are not greatly influenced by possible imperfections at the surfaces (vacancies, steps, kinks etc.) since the contours of both the positron-surface potential and the He-surface potential follow the electron density contours outside the surface in the present model. The changes in positron and He densities induced by surface imperfections therefore tend to match. Consequently, λ_{gas} will be relatively insensitive to details of the surface geometry. The results should therefore be applicable to a general Al surface as encountered in a He bubble.

One might on very general terms expect a relation between the positron lifetime and the He density qualitatively similar to the one for Al also for other metals. Helium profiles are mainly determined by the extension of the electron distribution outside the surface, i.e. the 'size' of the metal atoms, which for many metals is roughly the same, while the positron surface states at different metal surfaces also appear to be similar (same binding energy within about 1 eV [19]) suggesting positron-He atom overlaps for various interfaces to be similar. This notion was confirmed by a single calculation for the Cu-He system with $\bar{n}_{He} = 8.5 \times 10^{28} m^{-3}$, which showed a striking agreement with the Al-He results, e.g., $\tau = 298$ ps compared to the Al-He value of 300 ps calculated from Eq.(4.12).

In the theoretical description of the positron interface state employed, the positron-gas interaction is assumed to be unaffected by the metal electrons, since the gas atom positions are almost exclusively in the image potential region (distances from the topmost surface layer greater than about 2 A), where no accumulation of metal electrons around the positron occurs. In the 'physisorbed Ps' picture [50] of the positron surface state one would expect a stronger screening of the positron-gas atom interaction, and accordingly a smaller overlap leading to a lower λ_{gas} rather like an ortho-Ps pick-off annihilation rate [62] (see the discussion in chapter 8 for a description of Ps annihilation). In this picture it would be

difficult to account for the observed lifetimes without assuming unrealistically high gas densities in the bubbles. The image-potential model thus appears to provide a better description of the positron surface (interface) state in gas bubbles than the Ps model.

4.5. Positron calculations for vacancy-He clusters.

In the limit of small bubble sizes which generally corresponds to the highest He densities (cf. chapter 3) the positron interface state model inevitably breaks down. The positron will instead be in a volume state extending over the whole bubble volume. For this reason a separate set of calculations has been performed for small He-filled vacancy clusters (consisting of up to 13 vacancies) using the calculational method of Puska and Nieminen [51].

In most respects this method is similar to the one used for the interface calculations. The effective positron potential is calculated in the local-density approximation, Eq.(4.1), and the positron Schrödinger equation defined by this potential is solved numerically. The annihilation rate is then calculated using the local approximation Eq.(4.8). This implies that for the tightly bound core electrons (including those of the He atoms) the independent particle formula, Eq.(4.7), is used with γ equal to 1.5. The lower enhancement factor for annihilation with He electrons takes into account the stronger screening of the positron-He interaction by metal electrons in a small cavity compared to at a plane interface.

The He positions in the vacancy clusters were chosen so that the symmetry of the cluster was retained compared to the empty cluster while the He positions still appear physically sound (i.e. filling out the empty space of the vacancy cluster in a reasonable way). The requirement of symmetry is necessary to keep the unit cell of the positron calculation at a computationally manageable size. Exact He locations were determined by minimising the sum of Al-He and He-He interatomic interaction energies with respect to one or several parameters defining the He positions under the chosen symmetry restrictions. No relaxations of Al atomic positions were taken into account.

Examples of calculated wave functions in an empty and a He-filled cluster are given in Fig.11 and the positron lifetimes calculated for various combinations of vacancy and He numbers are presented in Fig.12. As expected it is found that the presence of He inside the cluster reduces the lifetime compared to the value for the empty cluster and that for a given He density (equivalent to a given ratio

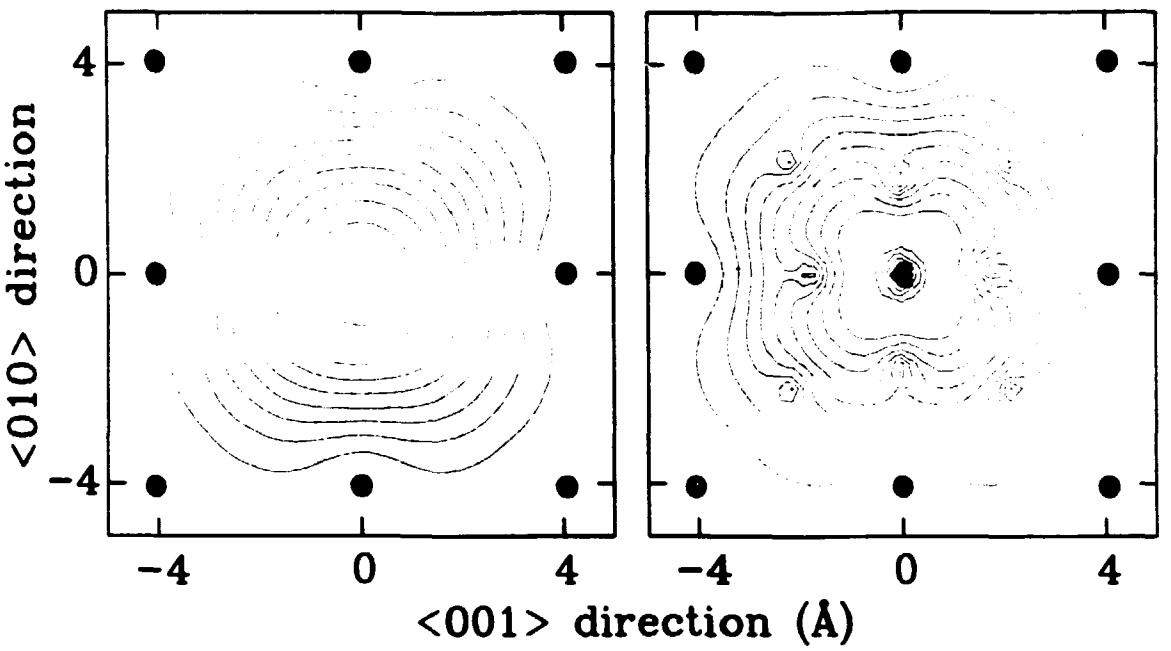

Fig.11. Calculated positron wave functions in an empty 13-vacancy cluster (left) and in a cluster of 13 vacancies and 27 He atoms (right), both in Al. In both cases the contour spacing is 1/10 of the maximum value. Al atomic positions are indicated by filled circles. The He positions in the right-hand part of the figure can be deduced from the dips in the wave function. Only 9 of the He atoms are in the plane of the figure.

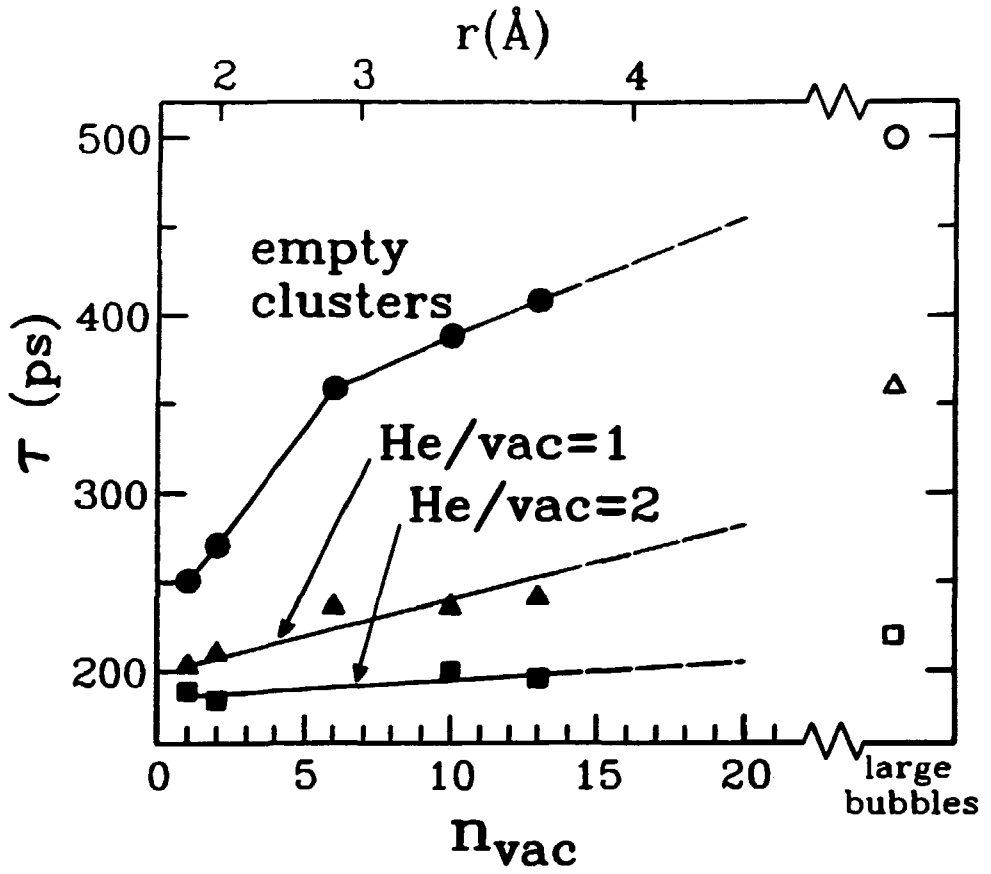

Fig.12. Calculated lifetimes in empty and He-filled vacancy clusters in Al grouped according to the He-vacancy ratio. The results are shown as function of the number of vacancies in the cluster, and the upper scale shows the corresponding cluster radius (calculated from the volume of the cluster). The open symbols at the right-hand side of the figure are results for large bubbles obtained from the Fig.10 relationship.

of He and vacancy numbers) the lifetime increases with cluster size and approaches the value for large bubbles calculated from the interface model. Only clusters with 13 vacancies or less are considered, since the image effects, eventually leading to the transition from a volume to a surface state for increasing cavity size, are not included in the cluster calculations. The 'intermediate' size region between the small cluster (volume state) and the large bubble (interface state) limits has not been examined because of the difficulty of accounting for the gradual transition between the local screening of the positron in the small cavities to the non-local image potential at the plane interface.

4.6. Comparison with experiment.

As will be described in the following chapters the present work includes an experimental study of 600 MeV proton irradiated Al containing He bubbles. The crosses in Fig.10 represent results from this study obtained for samples at their final stage of annealing where parallel positron annihilation and TEM examinations were made (see Paper I and chapter 6). The lifetime values are those of the most longlived component in the lifetime spectra. No direct determination of the He densities in the bubbles in the samples is possible but estimates have been obtained from the bubble sizes found by TEM by assuming the He pressures inside the bubbles to be in equilibrium (see chapter 3). Mean bubble diameters ranged from 40 to 100 A depending on the sample. In this size range the interface model of the positron state is appropriate.

The qualitative agreement between the two sets of points in Fig.10 is seen to be quite good. This firmly establishes the sensitivity of the positron lifetime to gas densities in bubbles.

In chapter 6 further evidence for the validity of the theoretical relation in Fig.10 is presented. This evidence relies essentially on the same results as gave rise to the crosses in Fig.10 but circumvents the equilibrium bubble assumption. The procedure is to evaluate the bubble radii and concentrations from the positron data and to compare the results to the independent TEM determinations of the same parameters. The positron results are indeed found to be consistent with the TEM data, providing strong support for the assumptions entering the analysis of the positron data including the theoretical lifetime-He density relation. The details of the experimental results are presented in chapter 6 and in Paper I.

It is difficult to obtain results by independent methods which allow

comparison with the positron calculations for the small vacancy-He clusters discussed in section 4.5. However, in a study of Al irradiated with He at low temperature Hansen et al. [63] argue from the known annealing behaviour of defects in Al that after annealing to a temperature of about 400 K, the defects observed to trap positrons must be vacancies or small vacancy-clusters containing He. The defect lifetime observed at this stage was 207 ps. This value is indeed consistent with the present calculations, since a 1 vacancy- 1 He cluster yields a lifetime close to this value. The increase in the defect lifetime observed upon further annealing at higher temperatures is consistent with the theory since it predicts a lifetime increase if the clusters coalesce and thereby increase their volume or if the clusters acquire vacancies and thus reduce the He-vacancy ratio. The experimental results of the present work allow no comparison with the small-cluster calculation since large bubbles had already been formed at the point where samples were investigated by positron annihilation.

4.7. Theoretical calculations for the Cu-Kr system.

A theoretical investigation similar to the one presented above for the Al-He system was also performed for the Cu-Kr system. These calculations were made to aid the interpretation of positron results on Cu and Ni containing 3-5 at. % Kr (see chapter 7). The details of the calculations are given in section III of Paper III.

The primary result is that it like for the Al-He system is possible to obtain a relation between the gas density inside bubbles and the lifetime of positrons trapped in the bubbles. This relation is shown in Fig.13. Like in the Al-He case the relation is approximately linear:

$$\tau(\text{ps}) = 500 - 92.3 \times \bar{n}_{Kr}(10^{28}\text{m}^{-3}), \qquad (4.13)$$

where $\bar{n}_{Kr}$ is the Kr density. The experimental point in Fig.13 has been obtained from Cu samples containing about 3 at.% Kr. In these samples Kr has been shown to be present in bubbles containing solid krypton at room temperature. The solidification is another manifestation of the high pressures which can exist inside gas bubbles (cf. chapter 3). The lifetime value of 257 ps is that of the longest lifetime component for the as-prepared samples. The corresponding density estimate has been obtained from the lattice parameter of the Kr lattice in the bubbles determined by electron diffraction [64] on samples similar to those used for positron measurements. This estimate should thus be fairly accurate. A density estimate based on the macroscopic swelling and the estimated Kr content of the samples gives

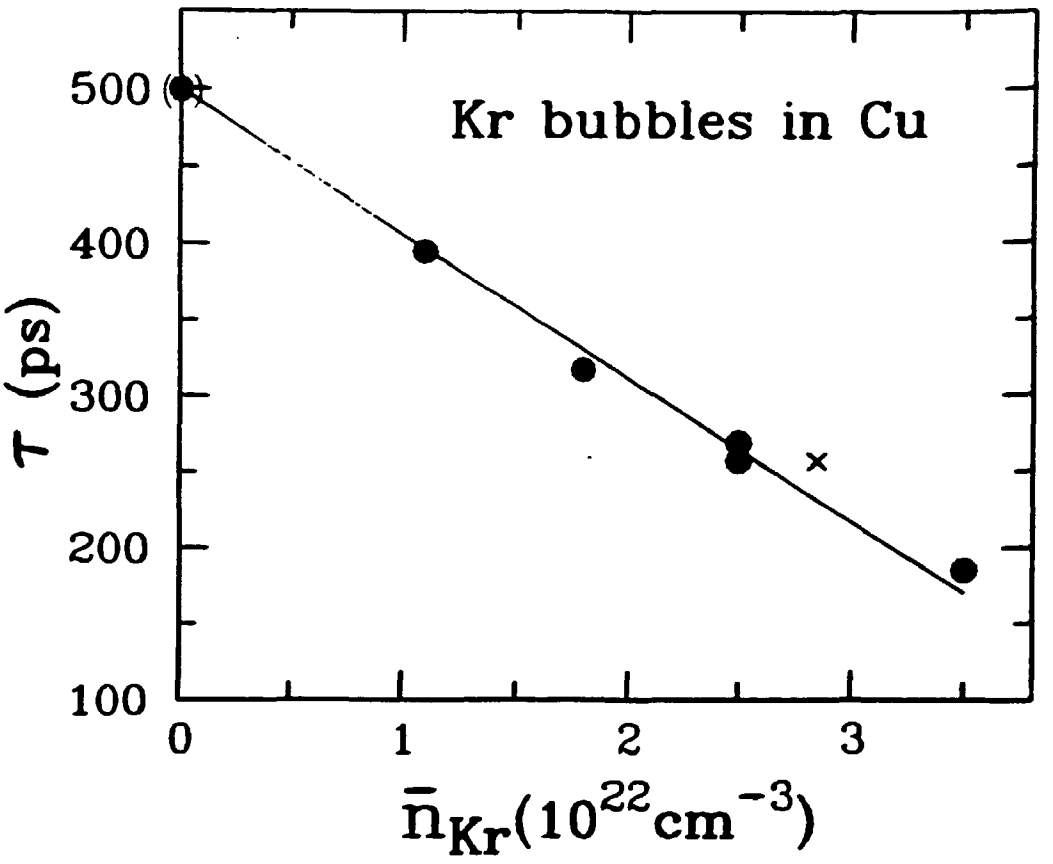

Fig.13. Positron lifetime as a function of Kr density in Kr bubbles in Cu at 300 K. Filled circles denote theoretical interface results. The line drawn is a visual fit. The cross is an experimental point for Cu containing ~3 at % Kr (cf. chapter 7).

approximately the same value [65]. The agreement between the theoretical lifetime-Kr density relation and the experimental result is encouraging.

Experimental results are available also for Kr in Ni (cf. chapter 7). On the same general grounds as was given above for the He case, one is led to expect the lifetime vs. Kr density relation for different metals to be similar. Comparison between the theory of Fig.13 and the experimental result for Ni-Kr, a lifetime of 243 ps compared to an estimated Kr density of 3.2×10^{28} m^{-3}, reveals a fair agreement supporting this idea.

5. DETERMINATION OF BUBBLE PARAMETERS FROM POSITRON RESULTS.

5.1. The trapping model.

Trapping of positrons into defects is often described in terms of the simple trapping model [66]. It assumes that positrons initially are in the bulk of the material where they annihilate with the rate $\lambda_b = \tau_b^{-1}$. From the bulk they may become trapped in a single type of defect with a time-independent trapping rate κ. For trapped positrons the annihilation rate is $\lambda_t = \tau_t^{-1}$. The transition rate from the trapped to the bulk state (i.e. the de-trapping rate) is assumed to be zero. Since estimated binding energies to traps such as vacancies and cavities are much larger than thermal energies, this presumbly is an accurate approximation. With these assumptions the disappearance of positrons from the bulk and the traps is governed by the rate equations:

$$dP_b/dt = -\lambda_b P_b - \kappa P_b \qquad (5.1a)$$

$$dP_t/dt = -\lambda_t P_t + \kappa P_b \qquad (5.1b)$$

where P_b and P_t are the probabilities that the positron is in the bulk and in a trapped state, respectively.

The solution of the rate equations results in a lifetime spectrum with two exponential decay components with the lifetimes

$$\tau_1 = (\lambda_b+\kappa)^{-1} \quad , \quad \tau_2 = \lambda_t^{-1} \qquad (5.2)$$

and relative intensities

$$I_2 = \kappa/(\lambda_b-\lambda_t+\kappa) \quad , \quad I_1=1-I_2. \qquad (5.3)$$

The model thus predicts a spectrum given by Eq.(2.6) on which the fitting analysis of lifetime spectra usually is based. The longlived τ_2 component is due to trapped positrons, while the shortlived component represents positrons annihilating in the bulk of the material. Because of the trapping into defects the bulk component lifetime is reduced from the value τ_b to the τ_1 of Eq.(5.2). This reduction in the observed bulk component lifetime is the most direct indication that the transition from the bulk to the trapped state occurs on a time-scale comparable to the positron lifetime. The trapping rate can be calculated from the experimental I_2 and τ_2 values using Eq.(5.3). The value of κ may then be inserted in Eq.(5.2) to obtain an estimate of τ_1. If this estimate agrees with the measured

τ_1, the experimental data are consistent with the trapping model.

The angular correlation curve measured for the sample will consist of a component with the shape of the curve for perfect bulk and a component due to the trapped positrons of intensity

$$N_2 = \kappa/(\lambda_b+\kappa). \qquad (5.4)$$

N_2 is equal to the fraction of positrons trapped before annihilation.

The above equations can easily be generalised to cases with more than one type of defect [66] (the equations for the two-trap case are given in Paper II).

Despite the extensive use of the trapping model in metal defects studies one should not forget that it is based on a number of assumptions, which may not always hold,e.g., the model does not account for trapping of positrons before thermalisation (prethermal trapping), which may be important in some cases [67]. In the next section the possible influence of time-dependence of the trapping rate into cavities, not accounted for by the model outlined above, will be discussed briefly.

5.2. Trapping rates into cavities.

Normally it is a good approximation that κ is proportional to the defect concentration C:

$$\kappa = \mu \times C \qquad (5.5)$$

where μ is the specific trapping rate. For cavities such as bubbles or voids μ will depend on the temperature and the defect radius r [20]. One of the objectives of the present work has been to establish the r-dependence of μ from the combined data sets from PAT and TEM for samples containing He bubbles or voids. A short account of these results has been published previously [68]. Figure 14 shows the results obtained. The filled symbols denote results for bubbles in proton-irradiated Al from the investigations presented in Papers I and II (except one of the circles which originates from results for a sample where the incident proton energy was 800 rather than 600 MeV [69]). The open symbols denote results for neutron-irradiated Al containing empty voids. The cross is the mono-vacancy result [71], while the straight continuous line for small r values is a theoretical line with a slope of 3 [72].

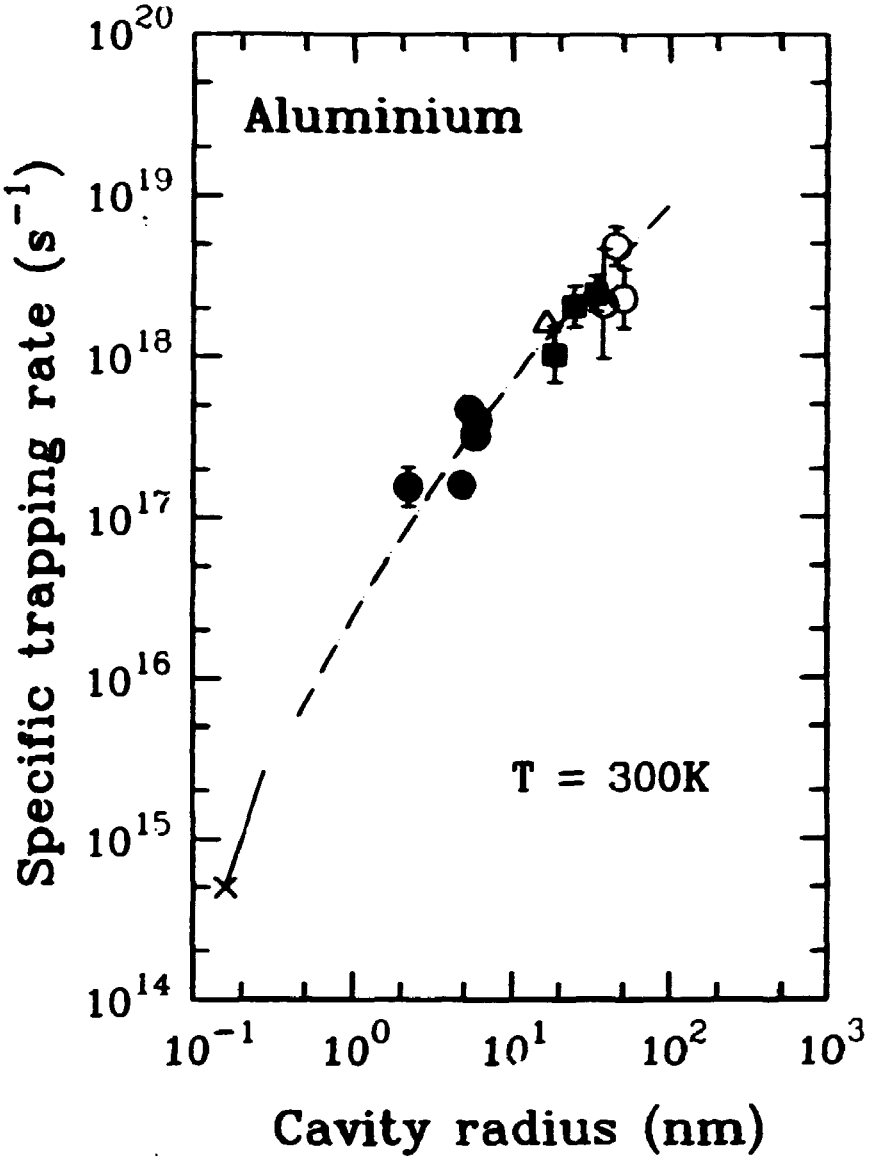

Fig.14. The specific trapping rate μ as a function of cavity radius for He bubbles (closed symbols) and for voids (open symbols): ● irradiated below 500 K and subsequently annealed (chapter 6 and ref. 69), ■ as-irradiated at about 700 K (chapter 8), O as-irradiated (below 400 K), Δ from ref. 70. The cross indicates the mono-vacancy result [71]. The straight line for small values of the radius is a theoretical line with the slope of 3 [72]. The broken curve is drawn according to Eq.(5.6) to approximate the experimental data.

The dashed curve in Fig.14 has been drawn according to the equation:

$$\mu = (1/Ar + 1/Br^2)^{-1} \qquad (5.6)$$

with the constants A and B adjusted to 9.07×10^{15} $A^{-1}s^{-1}$ and 3.30×10^{14} $A^{-2}s^{-1}$, respectively, to make the curve agree with experiments at 150 A and the theory at 3 A. The curve clearly reproduces the trend defined by the experimental points with a r^1 dependence for large r and a r^2 dependence in the intermediate range around 5-50 A. The r^1 dependence corresponds to diffusion limited trapping [73], where it is the diffusion of the positrons in the bulk to the defect that governs the trapping rate. The constant A in the first term of Eq.(5.6), which represents the diffusion limited trapping, is given by $4\pi D\Omega$, where D is the positron diffusion constant and Ω the atomic volume of the metal [73]. The empirical constant A therefore implies a value of D of 1.2×10^{-4} m^2/s in fair agreement with previous estimates obtained from positron beam experiments [74] of $0.6\text{-}0.9\times10^{-4}$ m^2/s at 300 K. The r^2 dependence of μ is characteristic of transition limited trapping [73], where the trapping rate is determined by the quantum mechanical transition between the positron bulk state and the trapped state in the cavity. Eq.(5.6) is an approximate way of describing the transition between the regions of transition limited and diffusion limited trapping.

The trapping model assumes, as described in the previous section, that the trapping rate is time-independent. However, for the largest bubbles and voids considered in Fig.14 (radii of the order of 500 A) this may not be a good approximation. The reason is that the expression for the diffusion limited trapping rate:

$$\kappa_{diff} = 4\pi rDC\Omega, \qquad (5.7)$$

is valid only when a quasi-equilibrium positron density depleted at the edge of the trap has been attained. If the initial positron density is uniform, it takes a certain time for the quasi-equilibrium density profile to develop, and during this time the trapping rate varies (it decreases with time) [73, 75]. Eldrup and Jensen [76] have recently atttempted to evaluate how this effect influences the trapping rates estimated from lifetime spectra using the trapping model in the form presented in section 5.1. For bubbles with radii of the order of 500 A a significant deviation (of the order of 50%) of κ_{diff} from Eq.(5.7) is predicted, but for bubble radii of 50 A or less, which will be considered in chapter 6 and for which the framework exposed in the next section is intended, the effect of the time-dependence of the trapping rate is negligible.

5.3. Determination of bubble radii and concentrations.

The relationships between the positron lifetime and the He density inside bubbles and between the specific trapping rate and the bubble radius relate the measured positron results to the bubble characteristics. However, in order to obtain the bubble radii r and concentrations C from the measured positron data, i.e. the lifetime τ and the trapping rate κ, using these relationships, an additional assumption is required. This may either be the equilibrium bubble assumption, Eq.(3.2), or alternatively one might assume that all He within the sample is contained in the bubbles. If the total He concentration in the sample is N_{He} and all He is in the bubbles, one has

$$C = 3N_{He}/(4\pi r^3 n_{He}). \qquad (5.8)$$

Combined with Eq.(5.5) this leads to an equation:

$$r^3 = \mu(r) \cdot (3N_{He})/(4\pi n_{He} \kappa). \qquad (5.9)$$

With n_{He} from the lifetime-He density relation this equation may be solved for r if the function $\mu(r)$ is known, provided r is not in the region where $\mu(r)$ is proportional to r^3 (i.e. r<5 A). If one instead assumes the bubbles to be in equilibrium, r can be determined in a different way. The He density determined from the lifetime can be translated into a pressure inside the bubble via the equation-of-state and the pressure may in turn be related directly to the bubble radius by the equilibrium condition, Eq.(3.2). Once r is known C may be obtained from Eq.(5.8) (if N_{He} is known and all He is assumed to be in the bubbles).

For small bubbles τ depends on both n_{He} and r as noted in chapter 4 (cf. Fig.12). Similarly, μ, in addition to the r-dependence, is also affected by n_{He}, although the effect is expected to be minor (less than 25 % for the He densities considered here and largest for the highest He densities, see Paper III). These complications do not render the PAT method inapplicable, since no extra unknown is introduced into the set of equations. However, the complete $\tau(n_{He},r)$ and $\mu(n_{He},r)$ functions are not known at present.

The framework presented above will be used in the interpretation of the experimental results to be presented in the next chapter. As the bubbles in a sample generally have a size distribution of a certain width (implying also a distribution of He densities) the obtained values of n_{He} and r are to be interpreted as average values (although the precise character of these averages is left unspecified).

6. HELIUM BUBBLES IN 600 MeV PROTON IRRADIATED ALUMINIUM (LOW IRRADIATION TEMPERATURES).

6.1. Introduction.

In the previous chapter a framework has been presented which allows the evaluation of bubble characteristics such as radii, concentrations, and gas densities inside the bubbles from positron lifetime results. In the present chapter a series of experiments on Al samples which contain He bubbles as a result of being irradiated with 600 MeV protons is presented. By comparing the results obtained from the positron measurements with TEM results it is possible to test the validity of the procedures used in the interpretation of the positron results. In addition one-dimensional angular correlation curves for He bubbles with different He densities are determined. The details of the experiments are presented in Paper I.

6.2. Experimental.

The samples used were made from polycrystalline sheets, 0.09-0.12 mm thick, of 99.9999% pure aluminium. These sheets were irradiated with 600 MeV protons at temperatures between 375 and 485 K. The beam intensity profile was approximately elliptical Gaussian. Hence, by cutting the irradiated foil into a number of 3 mm discs along the major axis of the beam, samples with different average proton doses and dose rates were obtained. The irradiation doses ranged from 0.1 to 1.2 displacements per atom (dpa).

During irradiation He is generated in the samples through nuclear reactions. The ratio between the He deposition rate and the damage rate is about 215 ppm/dpa [77]. This means that the He contents of the samples range from about 25 to 250 ppm. A number of other impurities are generated as well [78]. The possible influence of these impurities on the positron results is discussed in section 6.3 of Paper I, where it is concluded that they do not affect the results substantially.

The material irradiated this way has been shown by TEM to contain bubbles with radii of the order of 10 Å at concentrations of 10^{22}-10^{23} m^{-3} [79].

A number of samples were isochronally annealed after irradiation, i.e. the samples were heated at a series of temperatures increasing in equidistant steps for a certain time at each temperature. The annealing was carried out in steps of ~50 K starting at 373 K with 30

min heating at each temperature in a vacuum better than 10^{-5} torr. Positron measurements at room temperature were made after each annealing step.

The positron lifetime experiments were made with a spectrometer with a time resolution FWHM of about 250 ps. Transmutation produced ^{22}Na in the samples acted as an internal positron source. The time resolution functions were determined from spectra measured for annealed (defect-free) Al using the program RESOLUTION (see chapter 2).

Because of the small thickness of the foils about half of the positrons escaped the samples. Therefore all measurements were carried out with the samples surrounded by annealed copper and the measured lifetime spectra were corrected for about 50 % annihilation in the Cu (lifetime 112 ps) in the POSITRONFIT analyses (see chapter 2).

Angular correlation (AC) measurements were made in the long slit geometry with an external ^{22}Na source (see chapter 2). Measurements were made at room temperature with an angular resolution of 1.4 mrad. The AC curves were analysed with the PARAFIT program.

The positron measurements were supplemented by transmission electron microscopy (TEM) investigation of some of the samples using a 100 keV electron microscope. Because TEM requires sample regions with a thickness of a few thousands of A, samples had to be thinned before examination. The samples were therefore unsuitable for positron measurements afterwards. This is the reason why TEM examination could only be performed after the conclusion of the positron mesurements for each sample.

6.3. Lifetime results.

The lifetime spectra for samples irradiated at temperatures below 418 K showed saturation or near-saturation trapping into traps with a positron lifetime of 300-350 ps, i.e. all or nearly all positrons were trapped before annihilation and the lifetime spectra consisted essentially only of a single component with a lifetime characteristic of the defects. These traps are interpreted to be He bubbles. According to Eq.(4.12) these lifetime values imply He densities of 6-8 $\times 10^{28}$ m^{-3}.

Since the trapping rates into the bubbles in the as-irradiated samples are either undetermined (due to saturation trapping) or very uncertain, the method represented by Eq.(5.9) cannot be applied to

derive bubble parameters from the positron data. Instead bubble radii were evaluated from n_{He} (obtained from Eq.(4.12)) assuming bubbles to be in equilibrium. This yielded values of around 10 A for the samples irradiated below 418 K. These bubble sizes are generally consistent with earlier TEM work on similar samples. The concentrations calculated via Eq.(5.8) (i.e. by assuming all He to be in the bubbles) were about 2×10^{22} m^{-3}. The earlier TEM work indicates that the true bubble concentration might be higher than the positron estimates by about a factor of three. However the positron estimates are very sensitive to inaccuracies in the various relations applied and the discrepancy is probably not significant (see further discussion in Paper I).

The defect lifetime observed for the sample irradiated at about 480 K was about 390 ps implying a lower He density in the bubbles than in the samples irradiated at lower temperatures. Evaluation of bubble parameters in the same manner as described above yielded results (radius 25 A, concentration 4.3×10^{21} m^{-3}) in good agreement with estimates based on earlier TEM work.

Isochronal annealing studies were made for four of the samples. In all cases no significant changes in the positron data were observed for annealing temperatures T_{ann} below 600 K. At higher T_{ann} the defect lifetime τ_2 increased while the intensity I_2 decreased (for the sample irradiated at ~480 K this did not happen until T_{ann} reached about 750 K). An example of this behaviour is shown in Fig.15. The increase in τ_2 infers a decrease in He density inside bubbles while the drop in I_2 indicates a decrease in bubble concentration. The lifetime value of the shortlived component was generally consistent with the value expected from the trapping model, cf. Eq.(5.2). The extraction of positron trapping rates from the lifetime spectra using the trapping model thus appears to be justified.

The positron data, τ_2 and κ, were used to compute bubble parameters as functions of annealing temperature using Eqs.(4.12), (5.9), and (5.8). When using Eqs.(5.8-5.9) it is assumed that all He is contained in the bubbles. Calculated values of radii, r_{PAT}, and concentrations, C_{PAT}, are presented in table 1 (reproduced from table 3 of Paper I). The uncertainties given for r_{PAT} and C_{PAT} correspond to estimated uncertainties of ~30 % on the quantity $N_{He}/\kappa n_{He}$ as well as on μ for a given r. It is seen that the agreement between radii and concentrations obtained by PAT after the final annealing and the corresponding TEM values is good when the bubble sizes are well within the TEM visibility range. The apparent disagreement for the sample denoted 418a indicates that there is a population of small bubbles

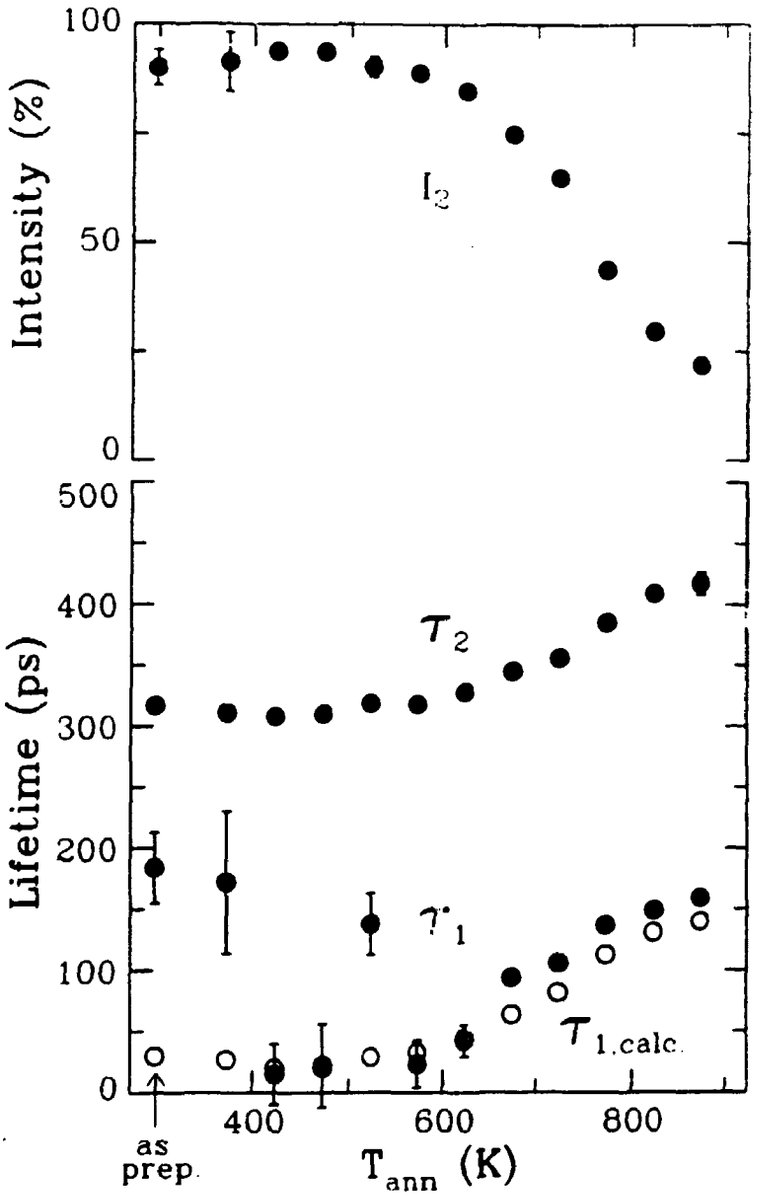

Fig.15. Lifetime results for Al sample irradiated with 600 MeV protons at about 380 K to a dose of 0.35 dpa (sample 395d) undergoing isochronal annealing as a function of the annealing temperature. Filled circles denote results from a two-component analysis of the lifetime spectra: lifetimes τ_1 and τ_2 and the relative intensity I_2. The error bars show the standard deviations obtained in the computer fitting analysis. The open circles show the expected values of the short lifetime, $\tau_{1,calc}$, calculated from the trapping model, Eq.(5.2).

Table 3. Helium density inside bubbles, n_{He}, bubble radius, r_{PAT}, and bubble concentration, C_{PAT}, estimated from the positron lifetime data for samples annealed at different temperatures T_{ann} (see text). τ is the lifetime of the bubble component and κ is the corresponding trapping rate. Results for T_{ann} lower than the values given in the table are similar to the first results given for each sample except for sample 418d where r_{PAT} and C_{PAT} cannot be calculated as κ is undetermined due to saturation trapping. The equilibrium bubble radius, r_{eq}, has been estimated from n_{He} and T_{ann}. The last two columns give TEM results obtained after completion of the PAT measurements.

T_{ann} (K)	τ (ps)	κ (ns^{-1})	n_{He} ($10^{28} m^{-3}$)	r_{eq} (A)	r_{PAT} (A)	C_{PAT} (m^{-3})	r_{TEM} (A)	C_{TEM} (m^{-3})
395d, 0.35 dpa, 75 appm He								
623	328	16.9	7.3	6	4±2	$(2.1\pm1.6)\cdot10^{23}$		
673	345	9.5	6.6	8	7±3	$(4.0\pm2.9)\cdot10^{22}$		
723	356	6.1	6.1	10	11±4	$(1.2\pm0.8)\cdot10^{22}$		
773	385	2.7	4.9	14	24±7	$(1.6\pm0.9)\cdot10^{21}$		
823	409	1.5	3.9	21	40±11	$(4.3\pm2.0)\cdot10^{20}$		
873	417	1.0	3.5	25	55±14	$(1.9\pm0.9)\cdot10^{20}$	60	$1.5\cdot10^{20}$
418a, 0.15 dpa, 32 appm He								
623	319	6.0	7.7	7	5±2	$(5.8\pm4.3)\cdot10^{22}$		
673	342	3.7	6.7	8	8±3	$(1.4\pm0.9)\cdot10^{22}$		
723	356	2.4	6.1	10	12±4	$(4.4\pm2.7)\cdot10^{21}$	22	$9.3\cdot10^{20}$
418d, 0.75 dpa, 161 appm He								
696	355	21.6	6.2	9	7±3	$(9.1\pm6.3)\cdot10^{22}$		
758	381	8.8	5.1	14	17±5	$(8.7\pm5.0)\cdot10^{21}$		
795	388	6.2	4.8	15	23±7	$(3.9\pm2.1)\cdot10^{21}$		
833	408	3.7	3.9	21	37±10	$(1.1\pm0.6)\cdot10^{21}$	48	$1.4\cdot10^{21}$
485b, 1.0 dpa, 215 appm He								
773	400	12-22	4.3	17	8-25	$(0.4-6.3)\cdot10^{22}$		
823	418	7-11	3.5	25	16-38	$(1.5-10.8)\cdot10^{21}$		
873	433	5.1	2.9	31	44±12	$(1.2\pm0.6)\cdot10^{21}$	58	$9.6\cdot10^{20}$

invisible in TEM but contributing to the PAT signal. Indeed, the size distribution observed by TEM for this sample extended down to the visibility limit of ~10 A radius, implying that the true bubble concentration might be higher and the mean radius lower than the TEM values given in the table. Given this fact, the conclusion is that the TEM and PAT results in Table 1 are mutually consistent in all cases.

Table 1 also includes r_{eq}, the equilibrium bubble radius, calculated assuming that the n_{He} values in the table represent equilibrium He densities at the annealing temperature. There is generally a good agreement between r_{eq} and r_{PAT}, but at the highest temperatures some deviations are observed, which could be explained if bubble sizes had changed during cooling of the samples from the annealing temperature and had equilibrated at a lower temperature.

6.4. Comparison with earlier studies of He bubbles in Al.

The present PAT results have been compared to earlier TEM work on annealing of bubbles in He-implanted Al, see Fig.16. Despite large variations in He concentrations and implantation energies in the TEM studies there is a good general agreement between the radii and concentrations observed after annealing of the samples at a given temperature. This agreement includes the results of the present study, where He has been introduced by transmutation reactions during proton irradiation rather than by direct implantation.

Aluminium in which He was implanted with 27 MeV energy has been the subject of an earlier positron lifetime study [39]. The defect lifetime for the as-irradiated sample, 360 ps, as well as the annealing behaviour in this study are very similar to the present results. This means that the defects acting as positron traps are specific to neither the proton-irradiated nor the He-implanted samples but are of the same type in both cases. The defects can be identified as He bubbles already by the agreement between PAT and TEM results for annealed samples in the present study, cf. table 1. However, the agreement between the measured positron data for the two types of specimens lends further support to this interpretation, since the bubble parameters derived from the positron data for proton-irradiated Al in the present work agree well with those found for He-implanted Al by TEM, cf. Fig.16.

The EELS method (see chapter 3) has been used previously to estimate He densities in bubbles in Al [85]. For bubbles with radius ~25 A a He density of 4×10^{28} m^{-3} was estimated. This value is consistent with

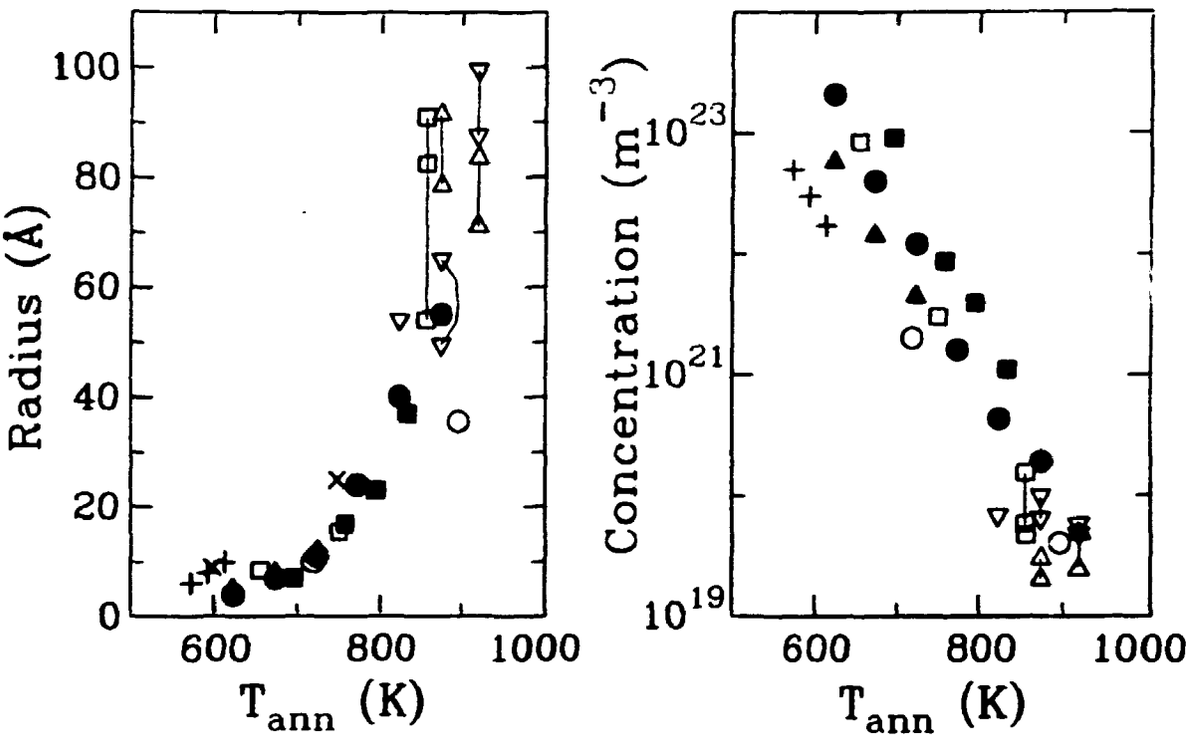

Fig.16. He bubble radii and concentrations in Al specimens annealed after introduction of He at lower temperatures. Filles symbols denote the present PAT results (table 1): sample 395d (circles), 418a (triangles), 418d (squares). Uncertainties are not indicated. Other symbols correspond to TEM data for He-implanted Al from the literature; open squares: 100 ppm, 70 MeV, 1 h (implant below 473 K) [80]; open triangles: 43 ppm (Δ) and 87 ppm (∇), 23 MeV, 1-1.5 h [81]; open circles: 4 ppm, 53 MeV, 1 h [82]; plusses: ~200 ppm, 20 keV, 5-10 min isochronal (implant at 573 K) [83]; crosses: 7.7 at.%, 0.5-8 keV, 20 min [84] (no concentration quoted). The numbers given above for each set of data are the He concentration, the implant energy and the annealing time. Data points connected by vertical lines correspond to different areas of a single specimen or different nominally identical specimens. Except where noted implantations were made below 400 K.

the densities estimated by PAT in the present work.

6.5. Angular correlation results.

In some of the as-irradiated samples the lifetime spectra indicate saturation trapping of positrons into He bubbles (see above). This means that the angular correlation curves for these samples (see Fig.17) supposedly correspond to the AC curves of positrons trapped in He bubbles. The measured lifetimes indicate different values of the He density in different samples. The difference between the measured angular correlation curves thus gives an indication of how the AC curves for He bubbles vary with He density. When the AC curves are analysed by the PARAFIT fitting program (see chapter 2), this variation can be expressed as changes in fitting parameters. Trial and error showed that the AC curves for the two samples with clear saturation trapping could be fitted with a sum of one parabola and two Gaussians and that only one of the fitting parameters (the width of one of the Gaussians denoted W_2) was significantly different for the two samples. This led to the conjecture that the AC curve for a general He bubble is given by the parametric description found for these curves with all parameters being constant except W_2 which allows for the difference in He densities.

The range of He densities for the as-irradiated samples were fairly limited. However, the annealing experiments allowed access to a wider range of densities. The lifetime experiments showed that in the annealed samples not all positrons were trapped before annihilation. The corresponding AC curves were therefore fitted as a sum of two components: one with the shape of the perfect bulk Al curve (representing un-trapped positrons) and one given by the parametric description for He bubbles mentioned above. All parameters describing the shape of the He bubble curve were constrained to fixed values except W_2 which was determined individually for each curve. The intensities of the two individual components were also determined separately for each curve. The AC results thus obtained were consistent with the independent lifetime results, since the intensities of the AC component agreed with the trapping model analysis of the lifetime spectra (see Fig.6 of Paper I) and there was a one-to-one correspondence within experimental accuracy between the two parameters reflecting the He density inside bubbles: the lifetime value and the parameter W_2 (see Fig.7 of Paper I). This consistency supports the conjecture, that the parametric description of He bubble AC curves mentioned above is valid within the whole density range observed in the bubbles in the present study. Figure 18 shows three examples of the curve shapes defined by this description.

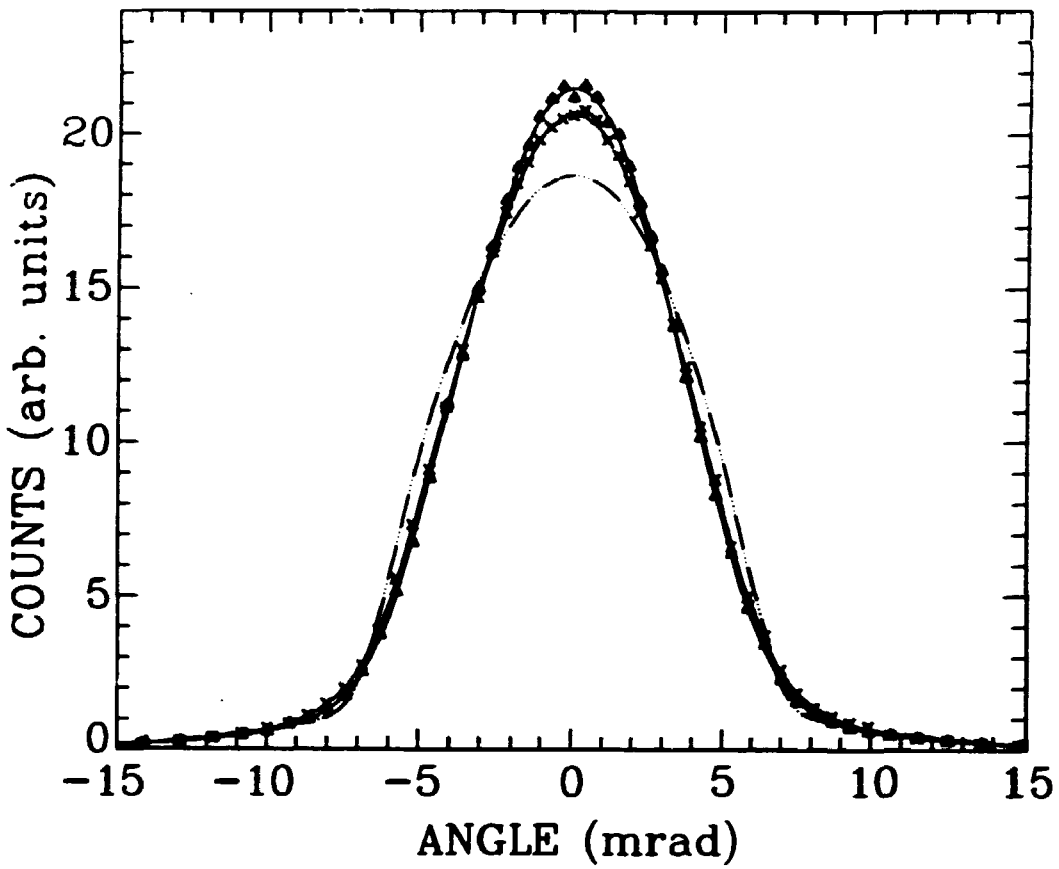

Fig.17. Measured angular correlation curves for 600 MeV proton-irradiated Al samples in the as-irradiated state: 395c, irradiated at 395 K to a dose of 0.6 dpa (crosses), and 418c, irradiated at 418 K to a dose of 1.21 dpa (triangles). The angular resolution is 1.4 mrad. Lifetime results indicate that all positron are trapped in bubbles before annihilation in these samples. The full curves have been obtained in the fitting analysis of the AC curves. For comparison the AC curve for bulk Al (Fig. 6) is shown as the dash-dotted curve. All curves have been normalised to the same total area.

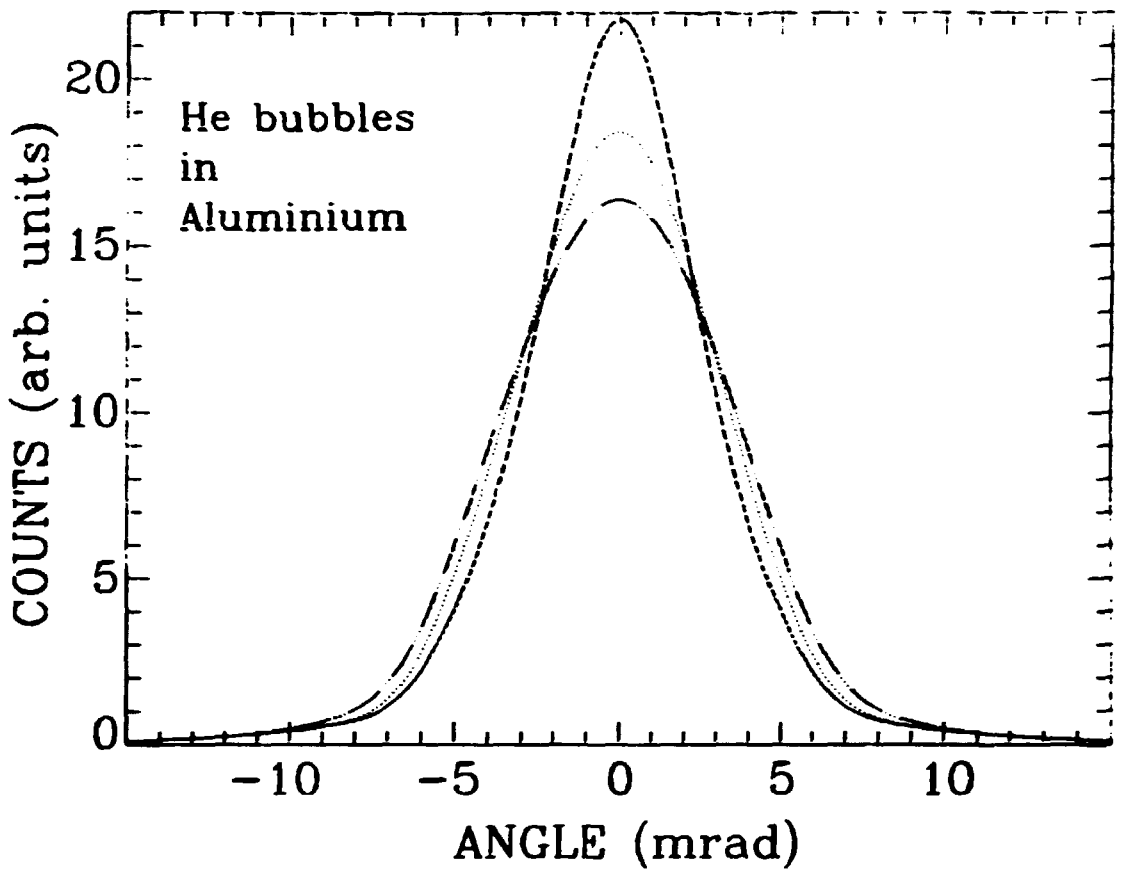

Fig.18. Angular correlation curves for positrons trapped in He bubbles in Al drawn according to the parametric description derived from the analysis of as-irradiated and annealed samples. The curves correspond to He densities (in 10^{28} m^{-3}) of 3.7 (dashed curve), 5.2 (dotted), and 7.4 (dash-dotted). The corresponding values of the parameter W_2 defining the shape are 4.5 mrad, 6.0 mrad, and 7.5 mrad, respectively.

The empirical AC curves for He bubbles presented here provides new information on positron annihilation in He bubbles. This information is relevant not only to future AC work but also to measurement of the Doppler broadening of the annihilation line (see chapter 2), which can be used both in conventional bulk experiments and in connection with positron beam techniques to study He implanted metals in the surface and near-surface regions [86-88].

7. COPPER AND NICKEL CONTAINING HIGH CONCENTRATIONS OF KRYPTON.

The present chapter contains a very brief account of the experimental studies of Cu and Ni containing high concentrations (a few at. %) of Kr. The results will mainly be discussed in relation to the connection between positron lifetimes and gas densities inside bubbles, while the detailed annealing behaviour of the samples receives less attention. No paper about these results is included in the thesis but they will be the subject of a future publication. Early accounts of the results can be found in refs. 89 and 90. Since the results for the Ni-Kr system do not qualitatively differ from those for the Cu-Kr system, only the Cu-Kr case will be discussed specificly.

The samples under study were prepared by the combined implantation and sputtering method developed at Harwell,UK as a means of storing radioactive ^{85}Kr from fission reactors [91]. By alternatively depositing Cu and implanting Kr thick (mm-cm) samples of Cu incorporating several atomic percent of Kr were produced. TEM examinations of as-prepared Cu-Kr samples [65] display a structure with small grains (size ~200 nm) dominated by a very high density (~5 $\times 10^{24}$ m^{-3}) of bubbles in the size range up to 30 A, the bubble distribution probably having a large submicroscopic component. The krypton inside these bubbles has been shown by electron diffraction to be in a crystalline state with a fcc structure [64]. The packing density of Kr in the bubbles is around 3×10^{28} m^{-3} implying pressures exceeding 1 GPa.

Positron measurements (both lifetime and angular correlation) were made both for as-prepared samples and in an isochronal annealing sequence.

The results emerging from the analyses of the lifetime spectra are shown in Fig.19. Up to an annealing temperature of 700°C the spectra could be resolved into two separate components, at higher temperatures into three components. In the first set of analyses, in which no constraints were imposed on the fitting parameters, the lifetime of one of the components (designated by index '2') scattered around a value of 180 ps throughout the temperature range without any detectable systematic variation. In order to reduce the scatter of the other parameters extracted, a second series of analyses was made with the lifetime of this component constrained to the value of 180 ps. The results shown in Fig. 19 are taken from this series.

The spectrum for the as-prepared samples consists of two components,

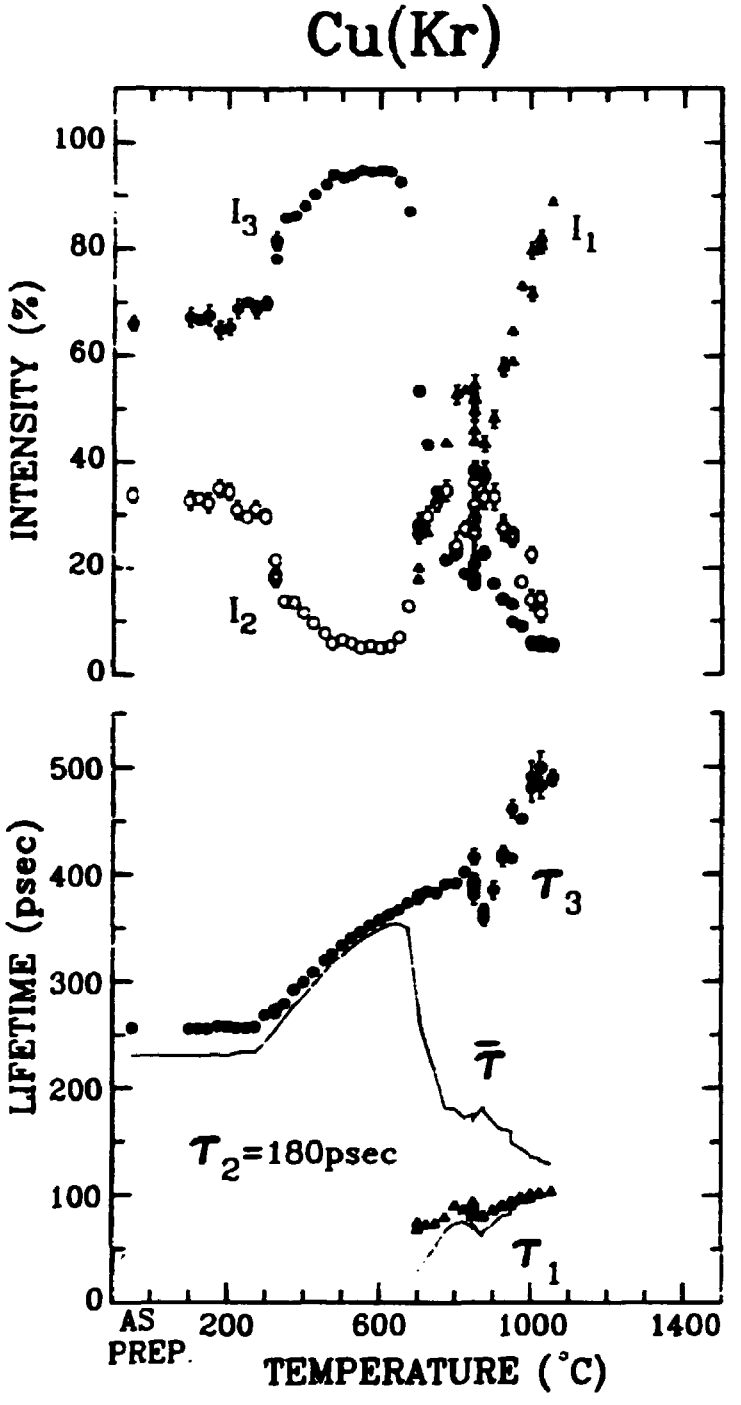

Fig.19. Positron lifetime results for Cu-Kr samples as a function of annealing temperature. At temperatures below 700 K the spectra are decomposed into two components with lifetimes τ_2 and τ_3 and corresponding intensities I_2 and I_3. At higher temperatures an additional component defined by τ_1 and I_1 were resolved. The value of τ_2 was fixed to 180 ps in all analyses. The full curve indicated by $\bar{\tau}$ shows the mean lifetime ($\bar{\tau} = \sum_i \tau_i I_i / \sum_i I_i$). The curve drawn close to the τ_1 points shows the τ_1 values expected from the trapping model (cf. Eq.(3.3) of Paper II, which is the two-trap equivalent to Eq.(5.2) of chapter 5).

both with lifetimes significantly larger than the bulk Cu lifetime of 112 ps. One is the above mentioned 180 ps component, while the other has a lifetime of 257 ps. The long lifetime indicates trapping in defects larger than single vacancies, which in Cu have a positron lifetime of about 180 ps. These defects presumably are the Kr bubbles. This interpretation is confirmed by the theoretical calculations described in chapter 4, since a lifetime value of 257 ps corresponds according to Eq.(4.13) to a Kr density, n_{Kr}, inside the bubbles of about $2.65 \times 10^{28}\ m^{-3}$ in good agreement with the estimate of $2.85 \times 10^{28}\ m^{-3}$ obtained from the lattice parameter of the Kr lattice inside the bubbles as determined from the electron diffraction pattern [64]. This estimate also agrees well with the n_{Kr} derived from the estimated Kr content (3.3 at.%) and the macroscopic swelling of the samples (determined from the mass density) [65]. The shortlived component either is due to a separate type of defect (single vacancies and dislocations both give rise to a lifetime around 180 ps) or it may indicate a distribution of lifetimes for the bubbles, e.g. because of a variation of the Kr density among the bubbles. If the latter is correct, then the estimate of the average Kr density presumably should be based on the mean lifetime ($\bar{\tau} = \sum \tau_i I_i / \sum I_i$) of 235 ps rather than on the longest lifetime. This, however, makes no significant change in the estimated n_{Kr} value.

In the isochronal annealing investigation of the samples no significant changes in the lifetime spectra were observed until a temperature of 300°C was reached. At this point the lifetime of the longlived component τ_3 started to increase. At the same time the intensity of the 180 ps component decreased almost to zero level. This could either signal the disappearance of the small Kr bubbles with the highest n_{Kr} or, if the 180 ps component is due to a separate type of defect, the annealing out of these defects. As temperatures were raised above 300°C τ_3 continued to increase reaching a value close to 500 ps after the final anneal near the Cu melting point. This indicates a gradual decrease of the Kr density inside the bubbles equivalent to the decrease of He density in the Al samples described in the previous chapter.

The decrease in n_{Kr} indicates an increase in bubble sizes. This bubble growth has been confirmed by TEM studies of similar material. The processes taking place presumably are migration and coalescence of bubbles together with loop punching or absorption of thermal vacancies (see chapter 3). The temperature of 300°C at which this growth is seen to start coincides with the temperature at which the solid Kr in the bubbles is observed to melt [64]. This might indicate that the migration and growth of bubbles is linked to this transition.

However, the correlation between the onset of bubble growth and melting of the Kr is less perfect for Ni-Kr although both temperatures (425 and 550°C, resp.) are higher than the corresponding Cu-Kr values.

The decrease in mean lifetime at 700°C coincided with a significant weight loss of the samples, whose values showed the loss of a major part of the Kr from the samples. Electron microscopy studies [65] have shown that in this temperature region the bubble coalescence processes cause large channels to be formed which then provide pathways to the surface for the release of gas. However a fraction of the krypton remains in the samples as indicated by the presence of a Kr bubble component also above 700°C. In the similar Ni-Kr material a thermal desorption measurement have shown that a Kr amount of the order of 200 ppm remained in the samples after annealing at a temperature close to the Ni melting point. Scanning electron microscopy showed that these Ni-Kr samples contained a large number of very big bubbles (radii of the order of 1-10 μm). Presumably the structure of the Cu samples near the melting point is similar to that of the Ni samples. The presence of the 180 ps component at high temperatures is presumably due to dislocations (the presence of dislocations was confirmed for the Ni case by TEM).

After the last anneal the lifetime spectrum of the Cu-Kr samples was measured as a function of the sample temperautre T. The lifetime of the longlived component in the spectra is shown in Fig.20. It is seen that the lifetime is constant with T around room temperature at a value of ~470 ps, but when T is lowered below about 250 K τ_3 starts decreasing approximately linearly with T reaching a value of ~300 ps at 10 K. The intensity of this component is 6-7 % decreasing gradually with increasing T.

The decrease in the lifetime upon cooling can be interpreted in terms of Kr adsorption on the surface of the bubbles. Refering to the electron microscopy examinations of the Ni-Kr samples, the Cu-Kr samples are expected to contain bubbles with sizes of the order of 1-10 μm althouth the exact range of bubble sizes is not known at present. The quoted size range corresponds to equilibrium Kr densities of the order of 10^{25}-10^{26} m^{-3} (assuming bubbles to have equilibrated at the annealing temperature), implying presssures at room temperature of 10^{5}-10^{6} Pa (1-10 atm.). These densities are too low to reduce the lifetime of a positron trapped in a bubble significantly below the value expected for an empty cavity of about 500 ps, cf. the measured value of 470 ps. However, when samples are cooled layers of Kr will start to adsorb on the bubble surfaces [92]. It can easily be shown that when bubbles are in equilibrium (cf.

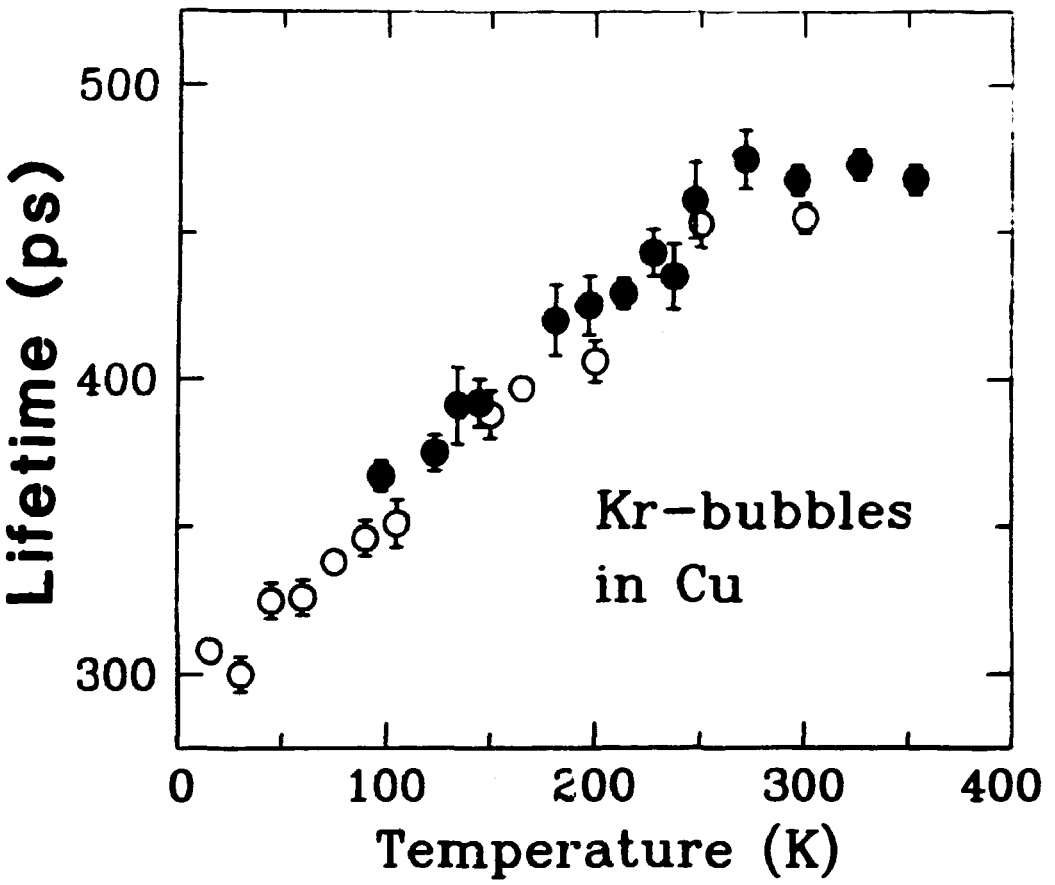

Fig.20. Lifetime of positrons trapped in Kr bubbles (i.e. the lifetime of the long-lived component in the lifetime spectra) in Cu-Kr samples annealed to 1128 K as a function of the sample temperature. Open and closed symbols correspond to results measured in two different setups.

chapter 3) the amount of Kr is sufficient to form several layers of adsorbed Kr on the bubble surfaces. The highest coverage that can be contained in a single Kr layer on a Cu surface is about 0.40. At higher coverages formation of second and subsequent layers has to take place. According to the theory of chapter 4 and Paper III, adsorption of 0.40 monolayer of Kr on a Cu surface reduces the lifetime of a surface trapped positron from about 500 ps to 300 ps (this point is discussed specificly in the section IV B of Paper III). Subsequent layers are expected only to have little effect on the lifetime. The temperature at which adsorption starts depends on the Kr density inside the bubbles [92, 93]. From the adsorption behaviour found experimentally for Kr on Cu(110) [94], Kr adsorption would be expected to start at about 200 K for a Kr density of 10^{26} m^{-3} (corresponding to 1 μm bubbles). This temperature coincides closely with the temperature at which the lifetime starts to drop. In larger bubbles with lower Kr density the adsorption starts at a lower temperature, e.g. for $n_{Kr} = 10^{25}$ m^{-3} (10 μm bubbles) the estimated adsorption onset temperature is about 150 K. When T is below 200 K it would thus be expected that in part of the bubbles the lifetime is decreasing towards 300 ps, while in others it is still close to the empty cavity value of ~500 ps. Because only a fairly small fraction of all positron are trapped in the bubbles (6-7%) it is not possible to resolve the bubble contribution to the lifetime spectra into more than a single component with a lifetime value determined by an average of the different lifetimes in the bubbles. According to this model one would therefore expect a gradual decrease of the lifetime as T is lowered below the limit where adsorption starts in the highest pressure bubbles. This agrees with the behaviour observed in Fig.20.

It should be noted that not all features of the results have been explained yet. There is no a priori reason to expect that the process described above should lead to a linear decrease in the lifetime but the linear behaviour may be fortuitous. It is also surprising that the lifetime decrease continues all the way down to the lowest temperatures. If there is an upper bound to the bubble sizes and thus a lower bound to the Kr densities inside (cf. the equilibrium condition) no further decrease in the measured lifetime should be measurable once the temperature has been lowered to the point where the first layer of Kr has condensed in the largest bubbles. However, the size distribution of the bubbles is not known at present. It is therefore not known at which temperature the lifetime decrease is expected to saturate. Electron microscopy investigations are planned in order to get more information about the samples. It should be pointed out however that the measured lifetime value at the low temperatures agrees well with the saturation lifetime of 300 ps

estimated theoretically (see above). In any case it seems clear that the observed effect is associated with Kr adsorption at the bubble surfaces. The results therefore give a direct indication of the location of positrons trapped in bubbles, since the decrease in the measured lifetime would be observed only if the positron is situated where the Kr goes, i.e. at the bubble surfaces.

8. POSITRONIUM-LIKE POSITRON STATES IN HELIUM BUBBLES.

8.1. Introduction.

In the preceding chapters positron trapping in noble gas bubbles has been discussed in terms of an interface-trapped positron model, where the presence of the gas gives rise to a reduction of the lifetime from the empty void value of ~500 ps to lower values. In the present chapter experimental evidence for a positron state of a different type in He bubbles is presented. Since the annihilation characteristics in certain respects resemble those of positronium (Ps) annihilation, this state will be referred to as Ps-like and the properties of the state will be discussed based on a positronium picture.

Since the first discovery of positron trapping in voids [95] the state of the positron in the voids has been a subject of considerable debate. The positron is now generally assumed to annihilate from a surface-trapped state [48]. The discussion in the previous chapters has been based on this picture. However, several authors have considered that formation of Ps inside cavities may take place [61,95-100]. Clear evidence for this proposal in the form of a very narrow component in angular correlation curves has previously been observed only for neutron-irradiated V and Nb [101]. The present chapter and Paper II present results for Al irradiated with 600 MeV protons at temperatures around 700 K (as opposed to the 400-500 K for the samples discussed in chapter 6 and Paper I) where a similar component is observed. The Ps-like states presumably are the results of impurities associated with the cavities. This point as well as the attempt to characterize the positron state based on the experimental evidence will be the subjects of this chapter.

8.2. Experimental.

In all major aspects the experimental details of the present part of the work is identical to those presented in chapter 6, the main difference being that samples were irradiated at temperatures around 700 K rather than the 400-500 K used for the chapter 6 samples. The higher temperatures mean that the bubbles created during irradiation are larger with radii of the order of 300 A and the He density inside the bubbles is lower, i.e. of the order of 5×10^{27} m^{-3}, than in the low-temperature samples.

8.3. Results.

The primary result for the present samples is the presence of a very

narrow component in the AC curves. An example is shown in Fig.21 which may be compared to the much broader curves for the He bubbles in the low-temperature samples shown in Fig.17. As will be discussed in more detail below this narrow component is a signature of a Ps-like state formed presumably inside the He bubbles. The FWHM of the narrow peak is about 1.6 mrad and depends only slightly on the irradiation dose received by the sample (cf. Fig.2 of Paper II) and the sample temperature (cf. Fig.3 of Paper II).

The lifetime spectra could be resolved into three separate components. The most longlived, which presumably is due to the He bubbles, had a lifetime of 480±30 ps. The intermediate component, which had a lifetime of 270-290 (±50) ps, may be ascribed to dislocations (see section 4.2 of Paper II for further discussion of this component). The shortlived component due to un-trapped positrons changed according to the trapping model as trapping rates into defects changed (cf. chapter 2).

The fraction of positrons annihilating in the 480 ps trap as calculated from the lifetime data using the trapping model was found consistently to be about a factor of 2 higher than the relative intensity of the narrow peak in the AC spectra, regardless of irradiation dose and sample temperature (see Fig.6 of Paper II).

8.4. Discussion.

The narrow AC component infers that part of the positrons annihilate from a state where the total momentum of the electron-positron pair is very low compared to normal electron momenta in metals. This indicates the formation of a bound positron-electron state with low centre-of-mass momentum. In insulators this type of state is frequently observed [102] and is referred to as quasi-positronium or simply as positronium, since the state has a number of properties in common with free positronium formed in vacuum. The discussion of the narrow AC component in the present work has therefore been made based on a positronium-picture of the positron state.

Positronium-like states are normally not observed in metals, since the conduction electron screening prevents the positron from being correlated to a single electron in a bound state [103]. Since the existence of Ps requires a low free-electron density [103] the narrow AC peak presumably is associated with positrons trapped in the He bubbles.

The AC curves for neutron irradiated Al containing voids do not

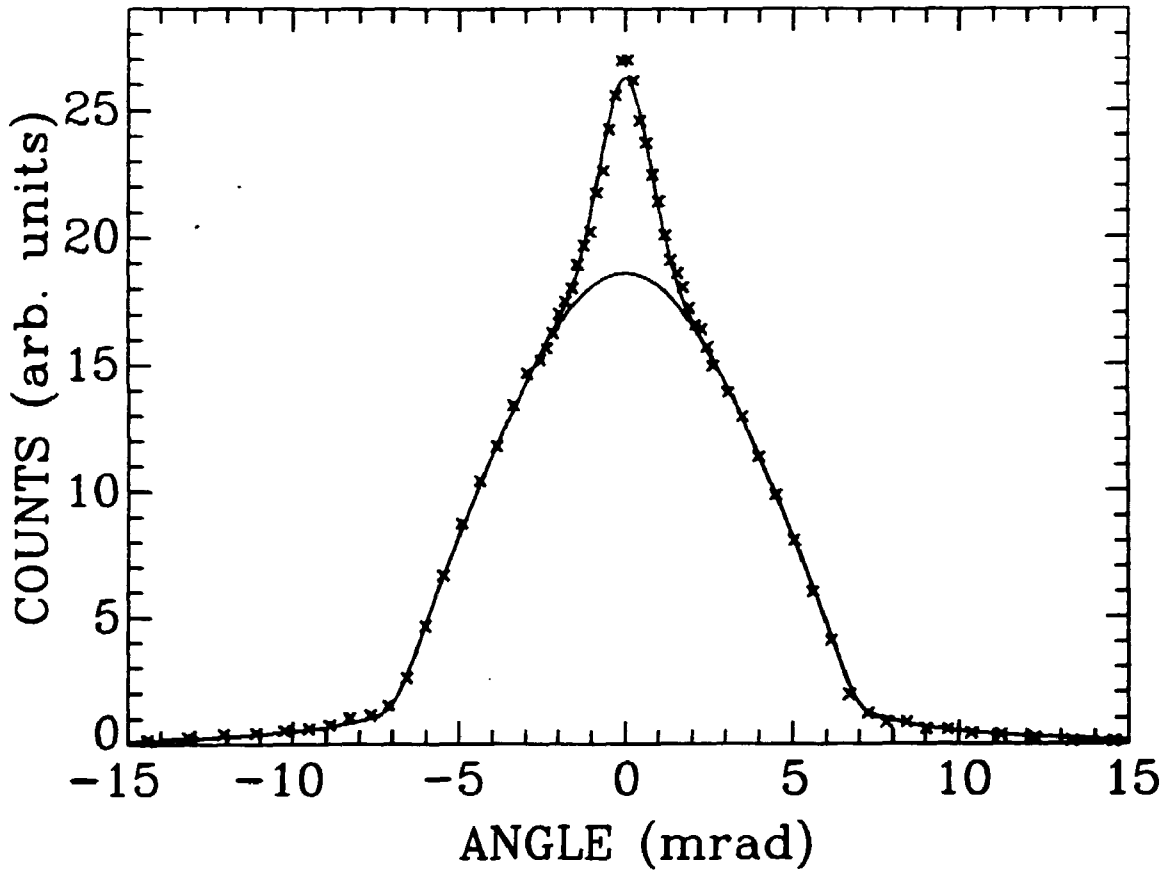

Fig.21. The AC curve for Al sample irradiated by 600 MeV protons at about 714 K to a dose of 1.1 dpa. The curve has been measured at room temperature with a resolution of about 0.4 mrad. The curve drawn through the points has been obtained in the computer fitting analysis of the spectrum. The lower curve shows the broad component of the curve detemined by this analysis.

contain narrow Ps components [96,100,104]. This is consistent with the fact that the positron surface state gives rise to a fairly broad (FWHM ~7 mrad) AC curve [27], and that positron beam experiments indicate that trapping of the positron in a surface state at a clean Al surface is energetically more favourable than formation of Ps. The latter is seen by the fact that it requires an activation energy of ~0.5 eV to desorb a surface-trapped positron as Ps [19]. Still, there is a certain probability that a positron reaching a metal surface from the bulk will be emitted as Ps [19]. However, even when positrons are emitted initially as Ps, the frequent interactions with the surface in a bubble or a void (it takes only ~1 ps for thermal Ps at 300 K to cross a 500 A cavity) probably leads to rapid dissociation of the Ps leaving the positron in a surface state. It thus follows that the Ps-like state in the He bubbles marks a departure from the clean surface situation. Because the noble gas-Ps interaction is dominantly repulsive (due to the electron-electron exchange interaction) [62] it is unlikely that the Ps-state is related to the He in the bubbles. Instead, the Ps-state presumably arises due to impurity atoms at the bubble surfaces. The possible nature of the impurity will be discussed later.

When Ps is formed it can emerge in either the para state (singlet, total spin 0) or the ortho state (triplet, total spin 1) [102]. The formation probabilities for the para and ortho states are 0.25 and 0.75, respectively, since there are three possible ortho states and only one para state. The binding energy difference (in vacuum) between these two states is only 8.45×10^{-4} eV (the hyperfine-splitting) [102]. In vacuum (and in the absence of magnetic fields) para-Ps annihilates by emission of two gamma-rays with a lifetime of ~120 ps while ortho-Ps decays by three-gamma annihilation with a lifetime of ~140 ns, i.e. about three orders of magnitude higher than the para-Ps lifetime. However, when Ps states are formed in condensed matter the ortho-Ps lifetime is reduced considerably because the positron can annihilate with an electron of the surrounding medium with anti-parallel spin. This is the so-called pick-off annihilation process [102]. Thus, typical ortho-Ps lifetimes in insulators are a few ns or less [102]. The above relates to the cases where the Ps when formed in either the para or the ortho state remains in this state until annihilation. However, the picture looks different when the Ps can exchange its electron with electrons of the surrounding medium with opposite spin. This spin-exchange process is normally only energetically possible in the presence of metallic electrons where empty states are available close to the Fermi level for both spin-directions. If the spin-exchange occurs frequently compared to the para-Ps annihilation rate, each Ps atom will spend about one

quarter of its time in the para state and the rest in the ortho state, because there is equal probability in each exchange process for the Ps to emerge in any of the four possible spin states. This means that almost all annihilations will take place from the para-state and the Ps lifetime is about four times the para-Ps lifetime, i.e. about 500 ps. The corresponding AC curve will be the narrow peak characteristic of intrinsic para-Ps annihilation [102] (unless some mechanism broadens the Ps momentum distribution, see below).

This picture is thus able to account for both the presence of the narrow AC peak and the lifetime value of about 480 ps. From the above one should expect a correspondence between the fraction of positrons annihilating in the 480 ps trap and the narrow peak intensity, but as noted previously there is a systematic ratio of about 2 between these quantities. There may be several reasons for this ratio. Since a lifetime of ~500 ps is also found for voids where no narrow AC peak is observed [59,60,61], there might be a contribution to the lifetime intensity from positrons annihilating from a state similar to the one in voids. Alternatively, the ratio of 2 could be an intrinsic property of the positron state in the bubbles (see below).

The width of the narrow peak shows that the Ps-like state is not just thermal Ps in the bubble interior since this would imply an even narrower AC component (see the discussion in Paper II). Presence of non-thermal free Ps in the bubbles appears unlikely since the frequent interactions with metallic electrons inferred from the spin-exchange would tend to thermalise the Ps. The broadening of the peak above the thermal FWHM could alternatively be due to localisation of the Ps, since the Ps zero-point motion would broaden the momentum distribution. Since the density of He inside the bubbles is too low to provide any localisation, the only possibility for localisation is at the bubble surface. The positron state might then be described as physisorbed Ps [50]. In this picture there might also be a contribution to the peak width from momentum transfer to non-annihilating electrons at the moment of annihilation (see the discussion in Paper II).

The physisorbed Ps model offers a possible explanation for the ratio of 2 between the positron fraction annihilating in the 480 ps trap and the narrow peak intensity, if the momentum distributions parallel and perpendicular to the bubble surface, whether caused by localisation or other mechanisms, are substantially different. In the AC curve such anisotropy could lead to a bubble component consisting of narrow and broad parts of roughly equal intensity. If the broad part had a sufficient width it would not be associated with the narrow bubble

component but rather be concealed within the other broad components of the AC curves. The narrow peak intensity would therefore only represent half of the bubble component while the lifetime component would correspond to the full intensity.

It has already been pointed out that the positron state giving rise to the narrow AC peak must be the result of the presence of impurity atoms at the bubble surface. A reduction in the electron work function, ϕ, generally favours Ps formation, as the Ps desorption energy may be expressed as $E_a = E_b + \phi - 6.8$ eV, where E_b is the surface state binding energy [19]. It is therefore likely that the impurity causing the Ps-like state is Na, since Na adsorption on an Al surface reduces ϕ considerably [105]. Na, produced by nuclear transmutations during the proton irradiation, is mobile in Al at the irradiation temperatures considered here [106]. Due to the extremely low solubility, Na is likely to segregate, possibly at the bubble surfaces. If all Na generated (~50 ppm/dpa) is adsorbed on the bubble surfaces, coverages of ~0.6 monolayer can be obtained. This would imply a decrease of ~1.6 eV in [105], i.e. larger than the E_a values for clean Al surfaces, 0.3-0.7 eV [19]. Positron beam results for alkali layers on Ni(100) [107] indicate that the decrease in ϕ may be accompanied by an increase in E_b nearly compensating the effect on E_a. However, it is not known whether a similar effect, preventing Ps formation, is found for Na on Al. Other elements than Na should also be considered since a multitude of impurities are generated during irradiation, although most of these are produced at lower rates than for Na [78].

The narrow peak is only observed for samples proton irradiated at high temperatures. For samples irradiated at 375-485 K no such component is present (chapter 6 and Paper I). The absence of the narrow peak for the low-temperature samples could be due to an impurity coverage of the bubble surface different from that in the high-temperature samples. This may be related to the fact that Na is mobile only above 500-600 K (the measured activation energy for Na diffusion in Al is 1.4 eV [106]). Annealing of the low-temperature samples at temperatures up to 873 K did not produce a narrow AC peak (Paper I). Thus, it was not possible to detect diffusion to the bubble surfaces of the impurity causing the AC peak. However, diffusion conditions under irradiation might be different from those under thermal annealing and the mobility of impurities could be impeded by binding to other defects such as small impurity clusters.

In order to substantiate the interpretation of the results presented above it clearly would be useful to perform positron beam experiments

on Al surfaces covered by adsorbates like Na. Such experiments would be able to test some of the hypotheses involved. However, the present results also suggest surface experiments which could be highly interesting in their own right. For example, if the conclusion regarding the different momentum distributions parallel and perpendicular to the surface is correct, one would observe a strongly anisotropic two-dimensional angular correlation curve for positrons on an external surface with a constitution identical to that of the He bubble surfaces in the present experiments. Such anisotropy would be quite unlike the almost isotropic curves measured for clean metal surfaces [27,28].

The results presented in this chapter is probably mostly interesting from the 'positron point-of-view', since it demonstrates the presence of a positron state which has been discussed frequently in the past but only observed in few cases before, and the interpretation suggests the state to be similar to the much debated 'physisorbed Ps' surface state. However, the results also contain information of relevance to defect properties, especially defect-impurity interactions, since the Ps-state implies the presence of impurities on the bubble surfaces. Such interactions have previously also been studied by the lifetime technique [108].

9. SUMMARY.

In the preceding chapters accounts of experimental and theoretical results from studies of noble gas bubbles in metals by positron annihilation have been given. The present chapter provides a broad summary of the major results, and the methods and results will be discussed within a wider context.

9.1. Summary of results.

The major new piece of information obtained from the combined set of results can be expressed as follows: The annihilation characteristics of a positron trapped in a noble gas bubble in a metal depends in a quantitatively predictable way on the density of gas inside the bubble. This conclusion emerges from the results of three individual parts of this work:

- a theoretical evaluation of the influence of the gas on a positron trapped at a noble gas-metal interface,

- experimental positron annihilation studies of Al samples in which He bubbles were present as a result of irradiation with 600 MeV protons, and

- experimental positron studies of Cu and Ni with a high concentration of Kr.

There is a good general agreement between the theory and the experimental results. For the Cu-Kr system the solidification of the Kr in the bubbles and the resulting diffraction pattern allowed a direct independent Kr density estimate to be made, and this was found to agree well with the one estimated from the positron lifetime data using the theoretical relation for the Cu-Kr interface system. For the Al-He system no such independent density determination was possible. Estimates were obtained from the equilibrium bubble condition which showed a fair agreement with positron lifetime estimates of the He densities. However, a better confirmation of the validity of the theory was obtained by using the positron data to evaluate bubble radii and concentrations, since a good agreement with TEM estimates could be obtained. It should be noted that the theory includes a number of adjustable parameters. However, none of these have been adjusted to He bubble data but to other experimental data such as bulk gas lifetimes and positron-gas atom scattering lengths.

The accordance between the theoretical predictions and the experiments

indicates that the model underlying the theory is basically correct. This means that the positron, as the theory predicts, is trapped at the metal-gas interface in a noble gas bubble. Only the plane-interface case was treated specificly in the calculations but it was argued that the effect of surface (interface) imperfections presumably would not have drastic effects on the results. However, it would be an obvious extension of the theory to examine the importance of imperfections. Similarly, it would be useful to calculate theoretical angular correlation curves which could be compared to those determined experimentally. Work is underway to do such calculations.

Theoretical calculations for positrons trapped in small vacancy-gas clusters were also made, supplementing the interface results applicable to large bubbles. Only the cases of large bubbles and small clusters were treated in the theoretical calculations. There is no obvious extension of the theory to make it include both the bubble size and He density effects on the positron annihilation characteristics throughout the whole size range, since it is difficult to account for the gradual transition between the local screening of the positron in small clusters and the image effects at the interface of a large bubble. To examine this problem in detail presumably a more sophisticated theoretical model is required which has sufficient power to account for the non-local many-body effects in the positron electron screening in a broad range of geometries.

The framework mentioned above is suitable for interpretation of the results for the Al samples irradiated with 600 MeV protons at temperatures below 500 K. In samples irradiated at around 700 K, the positron state in the bubbles is markedly different, in that a narrow component in the angular correlation curves indicates a positronium-like state, presumably a result of impurities (other than He) being present at the bubbles surfaces.

9.2. Evaluation of the positron method.

The present work has established that positron annihilation can yield a direct determination of the density of noble gases inside bubbles if bubble radii are above about 10 A (which may be known from previous experiments or it may be established by parallel TEM investigations). If the density information is combined with other data, determinations of bubble radii and concentrations can be obtained as well. At present a firm basis for the interpretation exists only for the lifetime method but angular correlation measurements possess a similar sensitivity to He densities. The AC method may even facilitate extension of the method to cover the complete range of bubble sizes.

The positron method is essentially non-destructive. This means that consecutive measurements can be made on the same samples after they have been subject to various treatments, e.g., annealing, between the measurements.

The conventional positron techniques (lifetime, AC, and Doppler broadening) are best suited for bulk measurements. Samples must have a certain thickness (for Al about 0.1 mm) to make sure that a major fraction of the positrons contributing to the measured signals annihilates in the region of interest. The lateral dimensions should be at least a few millimeters. These requirements put some limitations to the systems which can be studied. However, the use of bulk samples reduces the influence of extraneous effects due to the sample surfaces, e.g., in annealing experiments. When measurements of annihilation characteristics of trapped positrons in conjunction with positron beam techniques is established as a tool for defect studies, determination of defect characteristics as demonstrated in the present work will also become possible for thin films and for regions close to external surfaces.

The requirement of bulk samples makes the positron method suitable for studies of materials problems related to fusion reactor materials, since the 14 MeV neutrons which produce He penetrate deep into the materials and thus produce a defect structure extending over a considerable depth. In contrast most other methods used in He bubble studies generally require thin films of thicknesses of the order of μm.

In all positron lifetime studies the determination of the correct number of separate lifetime components in the measured spectra is a serious problem. If the component interpreted as being due to bubbles includes contributions from other unresolved components with lifetimes in the vicinity of that of the bubbles, the extracted information will be erroneous. The trapping model allows a consistency check to be made based on the value of the shortlived component, but this is generally not sufficient to assess the reliability of the analysis. In some cases annealing studies of the samples or measurements as function of temperature may be helpful in identifying the positron traps in a sample, since additional information about the defects is obtained. Whenever possible, independent examination of samples should be made by other methods such as TEM, which may test the validity of some of the predictions made based on the positron data. The uncertainties inherent in the spectrum analysis motivate the continuing development of lifetime spectrometers with better resolution and higher detection efficiencies which facilitate reliable

interpretation of the lifetime spectra. The amount of information which can be extracted with present-day spectrometers means that averages of parameters like gas densities and bubble sizes can be obtained, whereas little can be said about the variation of these quantities among the bubbles in a sample.

The positron method is sensitive to bubbles regardless of their size, from vacancy-He pairs to μm-sized bubbles, but the lower concentration limit of course depends on the cavity size. It is in general reasonable to assume that a bubble component of intensity ~2 % can be resolved from an otherwise perfect bulk metal spectrum. For 10 A bubbles this implies a detection limit of $\sim 10^{21}$ m^{-3}, for 100 A bubbles the limit is $\sim 10^{19}$ m^{-3}. If the bubbles contain He and are in equilibrium these limits imply overall He concentrations of the order of 1 ppm. It is thus seen that positron annihilation is sensitive to bubbles even when gas concentrations are fairly low. The He production rates in future fusion reactors are estimated to be about 100 ppm/year [7]. This means that the He concentration range where the positron method is most suitable is also the most important in relation to the fusion reactor materials problems. Most other methods which can yield density information such as EELS generally require much higher He contents of the samples, typically concentrations of several atomic percent.

10. CONCLUSION.

The present work has provided an experimental and theoretical analysis of positron trapping in noble gas bubbles. New insight into the nature of the positron state in the bubbles has been obtained, and the influence of the gas atoms on the positron state and the measurable annihilation characteristics were established.

The importance of these results and the impact on future research depends on the extent to which the positron method will be used for gas bubble studies. However, gas bubbles in metals is a topic of growing interest and the demonstration in the present work that it is possible to obtain quantitative information about bubble properties such as the gas density should encourage further use of the positron technique in these studies.

REFERENCES

1. R.N. West, Positron Studies of Condensed Matter (Taylor and Francis, London, 1974), Adv.Phys. **22**,263 (1973).
2. Positrons in Solids, ed. by P. Hautojärvi (Berlin, Springer, 1979).
3. Positron Solid-State Physics, ed. by W. Brandt and A. Dupasquier (North-Holland, Amsterdam, 1983).
4. Positron Annihilation, ed. by P.G. Coleman, S.C. Sharma, L.M. Diana (North-Holland, Amsterdam, 1982).
5. Positron Annihilation, ed. by P.C. Jain, R.M. Singru, and K.P. Gopinathan (World Scientific, Singapore, 1985).
6. Proc. Int. Symp. on Fundamental Aspects of Helium in Metals, ed. by. H. Ullmaier, Radiat.Eff. **78**,1 (1983).
7. H. Ullmaier, Nuclear Fusion **24**,1039 (1984).
8. P. Hautojärvi and A. Vehanen, in ref.2 p.1.
9. S. Berko, in ref.3 p.64.
10. I.K. MacKenzie, in ref.3 p.196.
11. L.C. Smedskjaer and M.J. Fluss, in Methods of Experimental Phsyics vol.21, ed. by J.N. Mundy, S.J. Rothman, M.J. Fluss, and L.C. Smedskjaer (Academic Press, New York, 1983) p.77.
12. F.M. Jacobsen, Riso Report R-433 (1981).
13. M. Eldrup, Riso Report 254 (1971).
14. S. Linderoth, H.E. Hansen, B. Nielsen, and K. Petersen, Appl.Phys.A **33**,25 (1984).
15. P. Kirkegaard, M. Eldrup, O.E. Mogensen, and N.J. Pedersen, Comput. Phys. Commun. **23**,307 (1981).
16. W. Brandt, in ref.3 p.1.
17. P. Kubica and A.T. Stewart, Phys.Rev.Lett. **34**,852 (1975).
18. T. McMullen, in ref.5 p.657.
19. A.R. Mills, in ref.3 p.432.
20. R.M. Nieminen, J. Laakkonen, P. Hautojärvi, and A. Vehanen, Phys.Rev. B **19**,1397 (1979).
21. L.C. Smedskjaer, M. Manninen, and M.J. Fluss, J.Phys.F: Met.Phys. **10**,2237 (1980).
22. P. Hautojärvi, J. Heinio, M. Manninen, and R.M. Nieminen, Phil.Mag. **35**,973 (1977).
23. R.M. Nieminen and M. Manninen, in ref.2 p.145.
24. A. Dupasquier and A. Zecca, Riv. Neuvo Cimento **8**,1 (1985).
25. D.A. Fischer, K.G. Lynn, and D.W. Gidley, Phys.Rev.B **33**,4479 (1986).
26. A.P. Mills and L. Pfeiffer, Phys.Rev.Lett. **43**,1961 (1979).
27. K.G. Lynn, A.P. Mills, R.N. West, S. Berko, K.F. Canter, and L.O. Roellig, Phys.Rev.Lett. **54**,1702 (1985).
28. R.H. Howell, P. Meyer, I.J.Rosenberg, and M.J. Fluss,

Phys.Rev.Lett. **54**,1698 (1985).
29. D.M. Chen, S. Berko, K.F. Canter, K.G. Lynn, A.P. Mills, L.O. Roellig, P. Sferlazzo, M. Weinert, and R.N. West, Phys.Rev. Lett. **58**,921 (1987).
30. K.G.Lynn, W.E. Frieze, and P.J. Schultz, Phys.Rev.Lett. **52**, 1137 (1984).
31. S.E. Donnelly, Radiat. Eff. **90**,1 (1985).
32. H. Trinkaus, Radiat.Eff. **78**,189 (1983).
33. T.R. Armstrong and P.J. Goodhew, Radiat.Eff. **77**,35 (1983).
34. J. Rothaut, H. Schroeder, and H. Ullmaier, Phil.Mag. A **47**,781 (1983).
35. E.E. Gruber, J.Appl.Phys. **38**,243 (1967).
36. P.J. Goodhew and S.K. Tyler, Proc.R.Soc.London A **377**,151 (1981).
37. A.J. Markworth, Metall.Transact. **4**,2651 (1973).
38. C.L. Snead, A.N. Goland, and F.W. Wiffen, J.Nucl.Mat. **64**,195 (1977).
39. H.E. Hansen, H. Rajainmäki, R. Talja, M.D. Bentzon, R.M. Nieminen, and K. Petersen, J.Phys.F:Met.Phys. **15**,1 (1985).
40. B. Viswanathan, W. Triftshäuser, and G. Kögel, Radiat.Eff. **78**,231 (1983).
41. B. Viswanathan, G. Amarendra, and K.P. Gopinathan, in ref. 5 p.862.
42. G. Kögel, Q.-M. Fan, P. Sperr, W. Triftshäuser, and B. Viswanathan, J.Nucl.Mater. **127**,125 (1985).
43. M.W. Finnis, A. van Veen, and L.M. Caspers, Radiat.Eff. **78**,121 (1983).
44. L.M. Caspers, A. van Veen, T.J. Bullough, Radiat.Eff. **78**,67 (1983).
45. K.O. Jensen and R.M. Nieminen, Phys.Rev. B **35**,2087 (1987).
46. M.W. Finnis and A.H. Harker, AERE Harwell Report 8824 (1983).
47. D.E. Sullivan, D. Levesque, and J.J. Weis, J.Chem.Phys **72**, 1170 (1980).
48. R.M. Nieminen, in ref.3 p.359.
49. R.M. Nieminen and M.J. Puska, Phys.Rev.Lett. **50**,281 (1983), M.J. Puska and R.M. Nieminen, Physica Scripta **T4**,79 (1983).
50. P.M. Platzman and N. Tzoar, Phys.Rev.B **33**,5900 (1986).
51. M.J. Puska and R.M. Nieminen, J.Phys.F:Met.Phys. **13**,333 (1983).
52. N.D. Lang and W. Kohn, Phys.Rev.B **7**,3541 (1973).
53. L.M. Schrader, Phys.Rev.A **20**,918 (1979).
54. H.E. Hansen, R.M. Nieminen, and M.J. Puska, J.Phys.F: Met.Phys. **14**,1299 (1984).
55. G.E. Kimball and G.H. Shortley, Phys.Rev. **45**,815 (1934).
56. E. Bonderup, J.U. Andersen, and D.N. Lowy, Phys.Rev.B **20**,883 (1979).

57. W. Brandt and J. Reinheimer, Phys.Lett. **35A**,109 (1971).
58. R.M. Nieminen, M.J. Puska, and M. Manninen, Phys.Rev.Lett. **53**,1298 (1984).
59. S. Linderoth, M.D. Bentzon, H.E. Hansen, and K. Petersen, ref.5 p.494.
60. K. Petersen, N. Thrane, G. Trumpy, and R.W. Hendricks, Appl. Phys. **10**,85 (1976).
61. V.W. Lindberg, J. D. McGervey, R.W. Hendricks, and W. Triftshäuser, Phil.Mag. **36**,117 (1977).
62. K. Rytsölä, J. Vettenranta, and P. Hautojärvi, J.Phys.B: At.Mol.Phys. **17**,3359 (1984).
63. H.E. Hansen, H. Rajainmäki, R.M. Nieminen, S. Linderoth, and K. Petersen, ref.5 p.512.
64. J.H. Evans and D.J. Mazey, J.Phys.F:Met.Phys. **15**,L1 (1985).
65. J.H. Evans, D.S. Whitmell, and R. Williamson, 12th Int. Symp. on the Effects of Irradiation on Metals, Williamsburg, USA (ASTM STP 870,1985) p.1225.
66. R.N. West, in ref.2 p.89.
67. T. McMullen and M.J. Stott, Phys.Rev.B **34**,8985 (1986).
68. K.O. Jensen, M. Eldrup, B.N. Singh, A. Horsewell, M. Victoria, and W.F. Sommer, Materials Science Forum, **15-18**,913 (1987).
69. M. Eldrup et al., to be published.
70. S. Linderoth, M.D. Bentzon, H.E. Hansen, and K. Petersen, in ref.5 p.494.
71. M.J. Fluss, S. Berko, B. Chakraborty, P. Lippel, and R.W. Siegel, J.Phys.F:Met.Phys. **14**,2285 (1984).
72. R.M. Nieminen and J. Laakkonen, Appl.Phys. **20**,181 (1979).
73. A.Seeger, Appl. Phys. **4**,183 (1974).
74. P.J. Schultz, K.G. Lynn, and B. Nielsen, Phys.Rev.B **32**,1369 (1985).
75. O.E. Mogensen, N.J. Pedersen, and M. Eldrup, in ref.5, p.756. O.E. Mogensen and N.J. Pedersen, Radiat.Phys.Chem. **28**,33 (1986).
76. M. Eldrup and K.O. Jensen, Proceedings of the European Meeting on Positron Studies of Defects, Wernigerode, 1987, to be published.
77. D. Gavillet, R. Gotthardt, J.L. Martin, S.L. Green, W.V. Green, and M. Victoria, ref.65 p.394.
78. S.L. Green, J.Nucl.Mater. **126**,30 (1984).
79. M. Victoria, W.V. Green, B.N. Singh, and T. Leffers, J.Nucl.Mater. **122-123**,737 (1984).
80. F.A. Smidt and A.G. Pieper, ASTM Spec.Tec.Publ. **570**,352 (1975).
81. H. Shiraishi, H. Sakairi, E. Yagi, T. Karasawa, R.R. Hasiguti, and R. Watanabe, Trans.Jap.Inst.Metals **17**,749 (1976).

82. K. Farrell, R.W. Chickering, and L.K. Mansur, Phil.Mag.A **53**,1 (1986).
83. K. Ono, M. Inoue, T. Kino, S. Furuno, and K. Izui, J.Nucl. Mater. **133-134**,477 (1985).
84. R. Manzke, G. Crecelius, W. Jäger, H. Trinkaus, and R. Zeller, Radiat.Eff. **78**,327 (1983).
85. W. Jäger, R. Manzke, H. Trinkaus, R. Zeller, J. Fink, and G. Crecelius, Radiat.Eff. **78**, 315 (1983).
86. G. Kögel and W. Triftshäuser, Radiat.Eff. **78**,221 (1983).
87. S. Tanigawa, Y. Iwase, A. Uedono, and H. Sakairi, J.Nucl.Mater. **133-134**,463 (1985).
88. K.G. Lynn, D.M. Chen, B. Nielsen, R. Pareja, and S. Myers, Phys.Rev.B **34**,1449 (1986).
89. M. Eldrup and J.H. Evans, J.Phys.F:Met.Phys. **12**,1265 (1982).
90. K.O. Jensen, M.Eldrup, and J.H. Evans, ref.5 p.506.
91. D.S. Whitmell, Radiat.Eff. **53**,209 (1981). D.S. Whitmell, R.S. Nelson, R. Williamson, M.J.S. Smith, and G.J. Bauer, European Appl. Res. Rept.-Nucl.Sci.Technol. **5**,513 (1983).
92. J.G. Dash, Films on Solid Surfaces (Academic, New York, 1975).
93. J. Unguris, L.W. Bruch, E.R. Moog, and M.B. Webb, Surf.Sci. **109**,522 (1981). J. Unguris, L.W. Bruch, M.B. Webb, and J.M. Philips, Surf.SCi. **114**,219 (1982).
94. A. Glachant, M. Jaubert, M. Bienfait, and G. Boato, Surf.Sci. **115**,219 (1981).
95. O.E. Mogensen, K. Petersen, R.M.J. Cotterill, and B. Hudson, Nature **239**,98 (1972). R.M.J. Cotterill, I.K. MacKenzie, L. Smedskjaer, G. Trumpy, and J.H.O.L. Träff, Nature **239**,101 (1972).
96. W. Triftshäuser, J.D. McGervey, and R.W. Hendricks, Phys.Rev. B **9**,3321 (1974).
97. P. Sen, L.J. Chen, and H.E. Kissinger, Phys.Lett. **53A**,229 (1975).
98. I.K. MacKenzie and P. Sen, Phys.Rev.Lett. **37**,1296 (1976).
99. P.J. Schultz, K.G. Lynn, I.K. MacKenzie, Y.C. Jean, and C.L. Snead, Phys.Rev.Lett. **44**,1629 (1980).
100. A. Alam, P.A. Walters, R.N. West, J.D. McGervey, J.Phys.F: Met.Phys. **14**,761 (1984).
101. E. Kuramoto, K. Kitajima, and M. Hasegawa, Phys.Lett. **86A**,311 (1981). M. Hasegawa, K.R. Hoffmann, R.R. Lee, S. Berko, and T. Takeyama, ref.5 p.260.
102. A. Dupasquier, in ref.3 p.510.
103. D.N. Lowy and A.D. Jackson, Phys.Rev.B **12**,1689 (1975).
104. K.O. Jensen, B.N. Singh, M. Eldrup, M. Victoria, and W.V. Green, Microstructural Characterization of Materials by Non-Microscopical Techniques, ed. by N. Hessel Andersen et al.

(Riso National Laboratory, 1984) p.333.
105. J.O. Porteus, Surf.Sci. **41**,512 (1974).
106. C.E. Ransley and H. Neufeld, J.Inst.Met. **78**,25 (1950).
107. A.R. Köymen, D.W. Gidley, and T.W. Capehart, in Proc. Int. Workshop Slow Positrons in Surface Science, ed. by A. Vehanen (Helsinki University of Technology Report 135, 1984).
108. H.E. Hansen, B.Nielsen, and K. Petersen, Radiat.Eff. **77**,1 (1983).

THANKYOUS

The work on which this thesis is based was performed primarily at the Chemistry and Metallurgy Departments of Risø National Laboratory. However, a major part of the theoretical work was done at the Department of Physics, University of Jyväskylä, Finland and a number of experimental measurements were made at the Laboratory for Applied Physics II, Technical University of Denmark. The final stages of the writing of the thesis were made at the School of Mathematics and Physics, University of East Anglia, UK. The hospitality and support at all these institutions are gratefully acknowledged.

Among the many persons I have interacted with during the work, I especially would like to thank my supervisor Morten Eldrup, Risø and Risto Nieminen, Jyväskylä without whom.... Thanks are also due to John Evans, Bachu Singh, Søren Linderoth, Michael Bentzon, Hannu Rajainmäki, Seppo Valkealahti, and Alison Walker for assistance and collaboration at various stages and for numerous discussions, to my second supervisor Jørgen Bøttiger for his support, to Finn Jacobsen for comments on the manuscript, and to Lone Jørgensen for efficient typing of the three preprinted manuscripts. Special thanks go to Niels Jørgen Pedersen for his indispensable technical and computational assistance.

LIST OF PUBLICATIONS

1. K.O. Jensen, B.N. Singh, M. Eldrup, M. Victoria, and W.V. Green, 'Helium bubbles in 600 MeV proton irradiated aluminium studied by positron annihilation', Microstructural Characterization of Materials by Non-Microscopical Techniques, ed. by N. Hessel Andersen et al. (Riso National Laboratory, 1984) p. 333-340.

2. K.O. Jensen, B.N. Singh, M. Eldrup, M. Victoria, and W.V. Green, 'Helium bubbles in 600 MeV proton irradiated aluminium studied by positron annihilation', Positron Annihilation, ed. by P.C. Jain, R.M. Singru, and K.P. Gopinathan (World Scientific, Singapore, 1985) p. 473-475.

3. K.O. Jensen, M. Eldrup, and J.H. Evans, 'Positron annihilation studies of copper and nickel containing high concentrations of krypton', ibid. p.506-508.

4. Kjeld O. Jensen, M. Eldrup, and B.N. Singh, 'Positronium formation in helium bubbles in 600 MeV proton-irradiated aluminium', J.Phys.F:Met.Phys. **15**, L287-L293 (1985).

5. K.O. Jensen, M. Eldrup, B.N. Singh, A. Horsewell, M. Victoria, and W.F. Sommer, 'Characterization of vacancy and vacancy-gas agglomerates in aluminium irradiated with medium energy protons by positron annihilation', Material Science Forum **15-18**, 913-917 (1987).

6. Kjeld O. Jensen and R.M. Nieminen, 'Helium bubbles in metals: Molecular-dynamics simulations and positron states' , Phys.Rev.B (Rapid Comm.) **35**, 2087-2090.

7. M. Eldrup and Kjeld O. Jensen, 'Trapping rates into cavities in Al: Temperature and size effects', Proceedings of the European Meeting on Positron Studies of Defects, in press.

8. Kjeld O. Jensen and R.M. Nieminen, 'Noble gas bubbles in metals: Molecular dynamics simulations and positron states', submitted to Phys.Rev.B (Paper III).

9. Kjeld O. Jensen, M.Eldrup, B.N. Singh, and M. Victoria, 'Helium bubbles in aluminium studied by positron annihilation: Determination of bubble parameters', to be submitted to J.Phys.F:Met.Phys. (Paper I).

10. Kjeld O. Jensen, M. Eldrup, B.N. Singh, S.Linderoth, and M.D. Bentzon, 'Positronium-like positron states in He bubbles in 600 MeV proton irradiated Al', to be submitted to J.Phys.F:Met.Phys. (Paper II).

11. Kjeld O. Jensen, M. Eldrup, N.J. Pedersen, and J.H. Evans, 'Annealing behaviour of copper and nickel containing high concentrations of krypton studied by positron annihilation', to be submitted to J.Phys.F:Met.Phys.

DANSK RESUME.

Positron-annihilations-teknikken (PAT) har i de senere år fundet en lang række anvendelser i studier af faste stoffer. I studier af metaller er det specielt PATs følsomhed for defekter såsom vakancer, vakanceclusters, voids og dislokationer, der er blevet udnyttet. Denne afhandling behandler anvendelsen af PAT til undersøgelse af en bestemt type defekter, nemlig ædelgas-bobler, d.v.s. gasfyldte kaviteter, i metaller. På grund af ædelsgassers uopløselighed i metaller opstår sådanne defekter, når ædelgasser introduceres i metaller, som f.eks. i fremtidens fusions-reaktorer, hvor neutroner, der undslipper fusionsplasmaet, vil danne helium i de omgivende materialer gennem (n,α)-reaktioner. Tætheden af gas inden i disse bobler kan være sammenlignelige med den atomare tæthed i metaller, hvilket implicerer ekstremt høje gastryk i boblerne, op til adskillige gigapascal. Dannelsen af bobler kan have en kraftig nedbrydende effekt på metallers materiale-egenskaber. Det er derfor vigtigt at udvikle eksperimentelle metoder til karakterisering af disse gas-bobler. Den mest direkte bestemmelse af størrelser og koncentrationer af bobler kan fås ved transmissions-elektronmikroskopi (TEM) under forudsætning af, at boblerne har en radius større end 10-20 Å. TEM giver normalt ikke information om indholdet af gas i boblerne. Hovedformålet med arbejdet, der er beskrevet i afhandlingen, er at bestemme tilstanden af en positron, der er indfanget i en ædelgas-boble, og at etablere, hvorledes gassen inden i boblen påvirker de målelige positron-annihilations-karakteristika, d.v.s. (middel-) levetiden af positronen og vinkelkorrelationskurven, der er fordelingen af vinkler mellem de to gammakvanter udsendt i annihilationsprocessen. Levetiden er et mål for elektrontætheden på positronens plads, og vinkelkorrelationskurven indeholder information om impulsfordelingen af de elektroner, positronen annihilerer med. Arbejdet er delvist eksperimentelt og delvist teoretisk. De teoretiske resultater er sammenlignet med de eksperimentelle og anvendt i interpretationen af disse resultater.

Den atomare struktur og positron-tilstande i ædelgas-bobler er behandlet teoretisk med Al-He og Cu-Kr systemerne som specifikke eksempler. Beregningerne for store bobler (radier over 10-20 Å) bygger på molecular-dynamics-simulering af metal-ædelgas-interfaces kombineret med positron-beregninger. Resultaterne demonstrerer, at positronen indfanges ved overfladen af boblen, d.v.s. ved metal-gas-interfacen. Annihilationsraten med metal-elektroner svarer til den ved en ren overflade, og der er samtidig en signifikant annihilationsrate med gasatom-elektroner. Dette muliggør etableringen af direkte relationer mellem gastætheden og positron-levetiden for de to systemer, der er anvendt som eksempler. Beregningerne indikerer, at bindings-

energien af positronen til metal-overfladen (d.v.s. interfacen) øges ved tilstedeværelsen af gasatomer. Molecular-dynamics-simuleringerne demonstrerer en tendens til tætpakket lagvis ordning af gasatomerne tæt ved metal-gas interfacen selv i de tilfælde, hvor gassen væk fra interfacen ikke er i fast fase. Positron beregningerne dækker også systemer, hvor enkelte lag af ædelgasser er adsorberet på metaloverflader, og har således også relevans for undersøgelser af ædelgas-adsorption ved hjælp af positron-beams. Komplementære positron-resultater for små vakance-ædelgas-clusters, hvor positronens bølgefunktion strækker sig over hele defektvolumenet, er præsenteret for clusters bestående af op til 13 vakancer. Tilstedeværelsen af gasatomer reducerer positronlevetiden i en cluster sammenlignet med værdien for en tom vakance-cluster af samme størrelse. For en bestemt gas-tæthed, d.v.s. et bestemt forhold mellem antallet af gasatomer og vakancer, stiger positron-levetiden som funktion af clusterens størrelse og nærmer sig levetiden bestemt ud fra interface-beregningerne for en stor boble med tilsvarende gastæthed.

Aluminium-prøver, hvori heliumbobler er introduceret gennem bestråling med 600 MeV-protoner, der danner helium ved kernereaktioner, ved temperaturer i intervallet 375-728 K, er undersøgt eksperimentelt med positron-annihilation. Både positron-levetidsteknikken og vinkel-korrelationsteknikken er anvendt. Prøverne bestrålet ved temperaturer under 485 K blev undersøgt både direkte efter bestråling og efter annealing ved temperaturer op til 873 K. Evaluering af bobleparametre, d.v.s. tætheden af gas inden i boblerne samt gennemsnitsradius og -koncentration, blev udført baseret på positron-resultaterne ved anvendelse af den teoretiske relation mellem gastæthed og positron-levetid samt en semi-empirisk relation mellem specifik positron-trapping-rate og radius af bobler. Det er således muligt at følge væksten af bobler under annealing. Væksten i boblestørrelse er knyttet sammen med et fald i bobletæthed. De opnåede resultater stemmer godt overens med bestemmelse af boble-parametre ved hjælp af andre eksperimentelle metoder, og resultaterne er konsistente med tidligere undersøgelser af aluminium, hvori helium er implanteret direkte snarere end introduceret gennem kernereaktioner. Variationen af formen af vinkelkorrelationskurven for positroner indfanget i bobler med tætheden af helium er bestemt ved at sammenholde resultaterne fra levetids- og vinkelkorrelationsmålingerne.

En meget smal komposant i vinkelkorrelationskurverne for prøverne proton-bestrålet over 655 K indikerer en positronium-lignende positron-tilstand i boblerne i disse prøver. Positronium er den brintatom-lignende bundne tilstand mellem en positron og en elektron. Bredden af denne komposant indikerer, at tilstanden ikke er frit positronium i boblernes indre, men snarere

en positronium-lignende tilstand ved boblernes overflade. Denne tilstand tilskrives tilstedeværelsen af urenhedsatomer, muligvis natrium, på overfladen af boblerne.

Eksperimentelle positron-levetids-resultater for kobber og nikkel, som indeholder høje koncentrationer af krypton, diskuteres kort. Estimater af Kr-tætheden i boblerne i disse samples baseret på de teoretiske resultater stemmer godt overens med uafhængige estimater. Måling af positron-levetiden som funktion af temperaturen for Cu-Kr prøver annealet tæt ved kobbers smeltepunkt demonstrerer effekten af adsorption af Kr på overfladerne af store bobler i prøverne på positron-levetiden i boblerne.

Riso National Laboratory **Riso - M - 2648**

Title and author(s)

Positron Annihilation in Noble Gas Bubbles in Metals

Kjeld Ole Jensen

Date November 1987

Department or group
Metallurgy

Groups own registration number(s)

Project/contract no.

Pages 94 Tables 3 Illustrations 21 References 108

ISBN 87-550-1325-2

Abstract (Max. 2000 char.)

An experimental and theoretical investigation of positron annihilation in noble gas bubbles in metals is presented.

A theoretical treatment of atomic structure and positron states in noble gas bubbles has been made. The Al-He and Cu-Kr systems are considered as specific examples. For large bubbles (radii above a few tens of A) a calculational scheme is developed combining molecular dynamics results for the metal-noble gas interface with positron calculations. It is demonstrated that a positron is trapped at the surface of a noble gas bubble, i.e. at the metal-gas interface, and relationships between gas density and positron lifetime were obtained for the systems considered. In the molecular dynamics simulations a trend towards close-packed layer-by-layer ordering of the gas atoms close to the metal-gas interface is found even in the cases, where the bulk gas is in a fluid phase. The positron state calculations also cover the case of adsorbed noble gas layers at surfaces. For small vacancy-noble gas clusters complementary positron results obtained with the calculational method developed by Puska and Nieminen are presented.

Aluminium samples containing He bubbles produced by 600 MeV proton irradiation at temperatures in the range 375-728 K were investigated experimentally by positron annihilation using both the positron lifetime and angular correlation techniques. The samples irradiated below 485 K were studied both in the as-irradiated state and after annealing at temperatures up to 873 K. Evaluation of bubble parameters, i.e. the gas density inside bubbles and the average

(continue next page)

Descriptors - INIS

ANGULAR CORRELATION; ANNIHILATION; BUBBLES; CAVITIES; CRYSTAL DEFECTS; HELIUM; KRYPTON; LIFETIME; METALS; MICROSTRUCTURE; POSITRONIUM; POSITRONS; PROTON BEAMS; TRAPPING; VOIDS

Available on request from Riso Library, Riso National Laboratory, (Riso Bibliotek, Forskningscenter Riso), P.O. Box 49, DK-4000 Roskilde, Denmark.
Telephone 02 37 12 12, ext. 2262. Telex: 43116. Telefax: 02 36 06 09

bubble size and concentration, were made from positron lifetime results employing the theoretical relation between positron lifetime and He density in bubbles and a semi-empirical relation between positron specific trapping rate and cavity radius. The results are consistent with determinations of bubble parameters by other experimental methods. In addition one-dimensional angular correlations curves for He bubbles as a function of He density are determined.

For the samples proton-irradiated above 655 K a very narrow component (full-width-at-half-maximum about 1.6 mrad) is present in the angular correlation spectra. This component is interpreted to be due to a positronium-like positron state in the He bubbles. The width of the narrow component indicates the state not to be free positronium in the bubble interior but a positronium-like state at the bubble surfaces. The Ps-like state is attributed to the presence of impurty atoms, possibly Na, at the surfaces of the bubbles.

Experimental positron lifetime results for Cu and Ni containing high concentrations of Kr are briefly discussed. Positron estimates of Kr densities inside the Kr bubbles present in the samples based on the theoretical results are consistent with independent estimates. Measurement of positron lifetimes as a function of temperature for the Cu-Kr samples after annealing close to the Cu melting point demonstrates the effect of Kr adsorption at the surfaces of the large bubbles present in the samples on the positron lifetime in the bubbles.

Available on request from
Risø Library,
Risø National Laboratory, P.O. Box 49,
DK-4000 Roskilde, Denmark
Phone (02) 37 12 12 ext. 2262

ISBN 87-550-1325-2
ISSN 0418-6435